Durham E-Theses

Observations and models of thermal emission from natural and man made objects

Ian David Roberts

How to cite:

Roberts, Ian David (1994) *Observations and models of thermal emission from natural and man made objects.* Masters thesis, Durham University.

Use policy

Abstract.

This thesis is concerned with the investigation of the measurement of radiometric temperatures of various terrestrial surfaces, and the implementation and validation of a number of mathematical models to represent and predict the thermal behaviour of such surfaces under various conditions.

Data can be acquired for radiation in a number of wavebands. Three radiometer systems built in Durham have been upgraded to allow measurements to be made in the 2-5μm and 8-14μm wavebands. The refurbishment of these systems is described.

An empirical model has been developed in Durham to describe the thermal behaviour of surfaces in terms of meteorological parameters. An experiment was carried out to determine the validity of this model for dealing with thermally light surfaces such as textiles. The analysis of the results from this investigation is presented.

Detection modelling involves the production of mathematical models to describe the behaviour of all components in a system, including the surface under observation, atmosphere and the detector. A number of published detection models are discussed, together with other models which describe the behaviour of one particular component, and which could be combined to produce a detection model for a particular purpose. One particular detector/atmosphere model, SenSAT-3, is the subject of a detailed evaluation, with a view to integrating it with the Durham General Purpose Model for surface temperature to produce a complete detection model.

The final chapter summarizes the current status of the work, and indicates possible directions for the future, including the development of a detection model based on the characteristics of the radiation thermometers installed in the Durham-built radiometers.

Observations and Models of Thermal Emission

from

Natural and Man Made Objects

by

Ian David Roberts, BSc.

A thesis submitted to the University of Durham in accordance with the regulations
for admittance to the degree of Master of Science.

Department of Physics   April 1994

University of Durham

Table of Contents.

Chapter 4 : An Empirical Model of Emission from Layered Surfaces

Chapter 5 : The Outline of a Detection Model

Chapter 6 : Evaluation of a Detection Model Package

Chapter 7 : Conclusions and Future Work

Appendices

Acknowledgements

Preface.

In conjunction with the Stores and Clothing Research and Development Establishment (S.C.R.D.E.), Colchester, Essex, Durham University has been involved in the development of radiometric data acquisition equipment, and the development and validation of models for thermal behaviour of surfaces since 1981. The author joined the group in October 1992.

Together with his colleagues, the author was involved in the refurbishment of three Durham-built radiometers on behalf of S.C.R.D.E.. The author's primary responsibilities included the commissioning of the radiation thermometers prior to installation in the upgraded system.

The author carried out the validation of the Durham Empirical Model for thermally light textile surfaces, as described in chapter four, in conjunction with other analyses performed by the group.

The author evaluated a commercial atmosphere/detector model package, to determine suitability for incorporation with the Durham General Purpose Model in a combined detection model. He also made preliminary investigations into converting the output from the detection model into a Probability of Detection model for a surface against some background.

None of the material contained in this thesis has been submitted previously for admittance to a degree in this or any other university.

Chapter 1. Introduction

1.1 Thermal Behaviour of Terrestrial Objects

All objects at temperatures above absolute zero emit long-wave infrared radiation. This radiation is a result of interactions between the object and its environment, and the re-radiation of absorbed short-wave radiation from the Sun. Long wave radiation in the approximate range $3 < \lambda < 30\mu m$ is emitted in the form of heat, and is thus described as thermal infrared (TIR) radiation. The radiation from objects at ambient temperatures (~300K) has a peak emission at wavelengths around 10μm. This coincides with a window from 8-14μm, in which the absorption of radiation by the atmosphere is relatively insignificant. This spectral region is also favoured by many constructors of radiation detectors due to the small solar contribution to the emission at such wavelengths. An alternative region of the electromagnetic spectrum used for thermal radiation observations is the short-wavelength infrared region (SWIR) which characterizes bodies at temperatures around 5000K, corresponding to wavelengths of approximately $1 < \lambda < 5\mu m$. This wavelength band is also relatively free from the effects of atmospheric attenuation, but is more affected by the short-wave solar flux.

The net radiative flux emitted at a surface is defined by the Stefan-Boltzmann law thus:

$$F = \varepsilon \, \sigma \, T^4 \qquad\qquad [\,1.1\,]$$

σ is the Stefan-Boltzmann constant ($5.67 \times 10^{-8} Wm^{-2}K^{-4}$).

T is the temperature of the body in degrees Kelvin.

1

ε is the emissivity of the surface, which is a function of the wavelength λ, and zenith angle of the incident radiation. The value of ε is in the range $0 < \varepsilon \leqslant 1$. $\varepsilon(\lambda) = 1$ for all λ defines a blackbody. $\varepsilon(\lambda) = k$ for all λ, with k non-unity defines a grey body, which is a suitable approximation for most natural objects. Most natural surfaces have emissivities in the infrared region between 0.90 and 0.95.

Since the function $\varepsilon(\lambda)$ is unique to any material, two different surfaces at the same temperature will emit different amounts of radiation at some fixed wavelength, and can thus be distinguished from one another.

Measurement of radiative flux can be expressed in a number of ways. The radiation temperature of an object is defined as the equivalent temperature required of a blackbody to emit the same flux in the waveband being measured. The physical temperature is higher than the radiation temperature for non-blackbody sources. The physical temperature can be measured by means of a contact sensor, or calculated from the radiative temperature if the emissivity of the surface is known.

1.2 Models for Prediction of Thermal Behaviour

The purpose of many numerical models is to provide an indication of the outcome of some procedure, without carrying out full scale measurements. Thus, an accurate model can save significant amounts of time and resources, and allow the investigation of a wider range of circumstances than might be possible in a measurement.

Models can be categorized by type, depending on the source of the data used as the model inputs. *Physical models* are derived from the general physical properties of the material and its environment. An example of such a model is the Durham General Purpose Model (Hughes *et al*, 1993) for thermal emission from natural and man-made objects. The accuracy of the predictions of these models can be verified by comparison with ground-truth experimental data. *Empirical models* are based on extensive sets of experimental data. The Durham Empirical Model (Turver, 1986) has been used to predict the temperature of an object on the basis of a number of input meteorological parameters. In cases such as this, the predictions of the model are based on the best fit to the archived radiometric dataset, but no consideration is applied as to whether the results have any physical significance. The parameters of the fit then allow predictions of the temperature of the same object based on different sets of meteorological data, characteristic of a different epoch.

Both of these models are discussed here.

1.3 Validation of Models

The development and validation of any thermal model requires the acquisition of a significant amount of radiometric and meteorological data. To this end, several Medium-Wavelength Infrared (MWIR) radiometers have been constructed at Durham. These were originally built to similar specifications with observing capabilities in the 8-14µm region of the electromagnetic spectrum. The prototype system was significantly upgraded in 1992, and two others were rebuilt in 1992-3. The modifications made to these units, and the testing and calibration of the sensors, will be described later.

1.4 Detection Modelling

The models described in section 1.2 deal only with the prediction of the temperature of the emitting object. Other models exist to deal with the effects of the atmosphere on infrared radiation transmission, and with sensor response. Examples of these latter models will be described with a discussion of different approaches to modelling the characteristics of the sensor. Packages are available which model the combined effects of the sensor, atmosphere and emitting object. One such package is SENSAT-3, and this will be evaluated, with considerations of the construction of a generic detection model. Such a model links predictions of the behaviour of an emitting object with the effects on signal propogation of the atmosphere and the response of the sensor, and can provide a measure of the probability of detection for a given object against some background. The development of a detection model based on the Durham models and the specification of the radiometers in use at Durham will also be discussed.

1.5 Scope of this Thesis

A number of models have been published which describe the thermal properties of surfaces under different meteorological conditions. This thesis contains a discussion on the different types of models available, and a description of the equipment used to validate the results of these models. Analysis of measured data is included to demonstrate the validation of one such model, the Durham Empirical Model, for use in predicting the emission from layered textile surfaces. This represents a more challenging application of the model than previous cases.

The concept of remote temperature measurements means that factors other than the emitter may influence the signal recorded by the detector. Atmospheric attenuation effects must be considered, and will be significant for long ranges between emitter and sensor. The characteristics of the detector, such as the spectral sensitivity at different radiation wavelengths must also be considered. The combination of these effects can be simulated by constructing a *Detection Model*.

The construction of a generic model for detection comprising a physical model for the emitter and a package (SenSAT) will also be outlined, and the SenSAT package will be evaluated.

Chapter 2. Previous Models and Observations

2.1 Introduction

The ability to understand and predict the thermal response of an object to changes in its environment has numerous applications. To this end a number of models have been produced to predict the temperature of some surface on the basis of a number of externally measurable variables. A successful model of this form will allow the temperature of an object to be influenced, with applications in, for example, military camouflage and concealment devices, satellite remote sensing and the monitoring of areas of agricultural crops. It will also allow the prediction of the thermal behaviour of an object at some time in the future from an initial set of measurements.

In Durham, three models for the thermal behaviour of an object or surface have been developed. Two of these, the Durham General Purpose Model (DGPM, Hughes *et al,* 1993) and the Durham Snow Model (DSM, McComb *et al,* 1992) are physical models, and make predictions of temperature based on the physical properties of the object material, and the prevailing meteorological conditions. The third is an empirical model. This model also produces estimates of temperature from the current meteorological conditions, but makes no direct consideration of the characteristics of the material. Instead, a `best-fit' representation of observational data is produced by using linear regression techniques to fit the model to these data.

In this chapter, these three models are described, together with a discussion of the requirements for validating the models.

2.2 Physical Models For Thermal Emission

Radiative temperature measurement has many advantages over other direct methods of monitoring the temperature of a surface. Radiometric temperature measurement can be carried out remotely, whereas contact temperature measurements may not always be possible. It is also the only method to make a measurement of a temperature without disturbing/influencing the system. The use of contact thermometers involves the establishment of an equilibrium between the surface and the measuring device, which may have an effect on the temperature and physical condition of the object.

The two models developed in Durham to predict such radiative temperatures are both one-dimensional models, in that they are concerned with layered surfaces, where the only variation in structure is with depth; the first is a general model, the second deals with the special case of a layer of dry snow.

2.2.1 The General Purpose Model

The General Purpose Model (Hughes *et al*, 1993) was designed to predict the radiation temperature of the surfaces of natural and man-made bodies, over one or more 24 hour periods. The model is one-dimensional, and deals with the special case where the temperature of the body is constant at some depth below the surface. The model is therefore designed to be applicable to surfaces consisting of uniform horizontal layers, such as roads, airfield runways and unvegetated natural surfaces.

The model deals with the variation in temperature in an object between the surface, and a layer at depth h, where temperature remains constant throughout the period of the observation/modelling. Heat transfer through the object is represented

by means of conduction, and is defined by the equation of heat conduction:

$$\alpha . \frac{\delta^2 T(z,t)}{\delta z^2} = \frac{\delta T(z,t)}{\delta t}$$

[2.1]

where α is the thermal diffusivity,

T is the temperature at time t,

z is the depth below the surface.

This equation is uniquely soluble if two boundary conditions are supplied. These are:-

(i) At some depth, the temperature is held constant.

(ii) At the surface, the net heat flux G is defined by:

$$\left. \frac{k.\delta T}{\delta z} \right|_{z=0} = G$$

[2.2]

where k is the thermal conductivity of the material, and the derivative $\delta T/\delta z$ is the temperature gradient at the surface. The values of the heat flux acting at the surface must balance, requiring:

$$S + R + H + L + G = 0$$

[2.3]

where S is the absorbed short-wave solar flux,

R is the net absorbed long-wave solar flux,

H is the sensible heat flux,

L is the latent heat flux.

The form of this equation is central to the development of the model, and is dependent on the meteorological conditions at the surface.

The incident solar flux is the dominant feature in most physical processes occurring in object-atmosphere systems, and the model uses established methods to

predict the solar flux, with additional corrections to allow for the position of the sun and the orientation of the object. The effect of cloud-cover is important; it is modelled by assuming that clouds cut out some fraction C of the incident flux. Look-up tables are available for values of C for various cloud types. However, McComb *et al* (1992) concede that, particularly where cloud cover is a concern, predictions of incident solar flux may be inaccurate. The alternative is to take measurements with a solarimeter. A fraction of this incident solar flux, defined by (1 - a), where a is the object albedo, is absorbed by the object. a *is a property of the material*, as well as a function of the zenith angle of the incident radiation. The treatment of long-wave radiation is more complex, since the object will be an emitter, and will also be receiving radiation reflected from its surroundings, as well as from the atmosphere.

Sensible heat flux is defined as the heat exchange across the boundary layer of still air immediately adjacent to the object, by means of conduction, and eddies in the atmosphere. The latent heat flux is associated with the evaporation or condensation of water on the surface. For both fluxes, empirical relationships are used in the model.

These factors are combined to calculate the heat flux into (or out of) the surface. The speed with which this heat flux reaches underlying layers is dependent on the thermal diffusivity of the material.

The model predicts the temperature profile of an object throughout a 24 hour period by approximating the heat conduction equation so that the temperature profile is given by the solution of a system of algebraic differential equations. Between the surface and depth z = h, the object is divided into a number of elements, each defined by three nodes (one in the middle and one at each end) at which the temperature is

known. By this method it is possible to use small elements where temperature change is greatest, and larger ones where small scale detail is unimportant. Elements can also be used to distinguish significant changes in the physical properties between layers, such as those made of different materials.

From the material structure and surface properties, the meteorological data, the time step Δt between datasets used and the initial temperature profile, the model may be used to calculate the surface temperature at time intervals Δt throughout a 24-hour period.

An analysis of the sensitivity of the model predictions to a range of parameters was carried out, to determine the effect of variation of each of the physical variables used on the output of the model. Each parameter was varied in turn, with the rest being held constant. The parameters to which the model is most sensitive, moderately sensitive and least sensitive have been inferred. The results are shown in Table 1 below, reproduced from the paper describing the Durham model. Within each group in the table, the most sensitive parameter is at the head of the list.

Most sensitive	Moderately sensitive	Least sensitive
Air temperature	Surface altitude	Wet and Dry bulb depression
Windspeed	Conductivity of top layer	Average ground albedo
Vertical emissivity		Surface atmospheric pressure
Vertical albedo		Conductivity of 2nd and 3rd layers
		Diffusivity of all layers
		Lower boundary conditions

Table 1. Summary of results of sensitivity analysis for DGPM

The validation of the model involved the comparison of predictions with physical data recorded for a number of objects. For the purpose of the validation, radiometric data for horizontal concrete and asphalt surfaces were considered. A weather station was used to record air temperature, solar radiation, windspeed and wet bulb depression. The thermometer used to acquire radiometric data was also used to take measurements of the sky temperature, for calculating the net long-wave solar flux. Data from a period free from precipitation were chosen for the validation, thus the surfaces were treated as being dry throughout the period, and the latent heat flux was set to zero. Published data were used for the surface parameters and conductivities and diffusivities of the materials. The results of the validation show that the model predicts temperatures in the range ±2°C of the physical data for most of the experimental period. Exceptions occur when cloud cover was present, when the absolute error increases, but the shape of the diurnal curves for predicted and observed temperatures remain similar.

In conclusion, it is noted that the model is particularly suitable for representing materials under cloudless skies, but the prediction is less accurate when clouds are present, due to difficulties in estimation of cloud type and extent of cover as the automated logging equipment was not ideally suited to the task.

2.2.2 The Durham Snow Model

Snow is a special case surface, and cannot be modelled using the DGPM due to the significant changes that occur in its structure due to relatively small changes in the thermal loading applied to it. Snow is also of a granular nature, and contains air and water vapour gaps between ice grains, through which heat exchange will occur, in addition to normal conduction processes through the solid ice.

Boundary conditions for the snow layer are defined in a similar fashion to those for the DGPM. The lower boundary is defined to have a time-independent temperature, and the temperature of the upper boundary is defined by equating the radiation fluxes acting at the surface.

The model is developed to predict the temperature at various depths within the snow layer, considering the extra heat-exchange processes due to the water vapour and air. A sensitivity analysis has been made, which identifies those parameters having the most significant influence on the model outputs. A summary of the results from this sensitivity analysis is reproduced from the paper in table 2.

Most Sensitive Parameters	Moderately Sensitive Parameters	Insensitive Parameters
Air temperature	Snow density	Snow conductivity
Moisture factor	Vapour diffusivity	Long wave emissivity
Windspeed	Snow depth	Albedo of soil surface
	Wet/dry bulb	Thermal properties of soil
	Surface altitude	Atmospheric pressure
	Drag factor	Lower boundary temperature
	Snow optical properties	

Table 2. Summary of results of Sensitivity Analysis for DSM

In conclusion, it is noted that the predicted snow temperature varies considerably with slight changes in surface air temperature and windspeed. The primary method of heat transfer within the snow layer is shown to be conduction due to the contact between grains, with heat transfer by vapour diffusion being unimportant except at

12

low densities ($\rho <$ ~300kg.m⁻³). McComb *et al* (1992) note the complexity of the system and stress the need for further, more exacting validation if the predictions of the model are to be accepted with confidence.

2.3 Empirical Models For Thermal Emission

A number of models exist which are not based on the physical properties of the material under observation. Such models may be produced by identifying the parameters which govern the temperature of an object either from observation or the predictions of a physical model. An extensive database including the measured radiative temperature of the object, together with comprehensive meteorological data covering an extended database must be assembled. The observed temperatures must be parameterized in terms of the quantities which govern the temperatures using non-linear fitting procedures. The strength, or otherwise, of such a model is dependent on the success with which it predicts temperatures for other periods of time with broadly similar meteorological conditions. One such model has been developed at Durham University and applied to a range of objects.

The Durham Empirical Model

Development of the Durham Empirical Model dates from 1978 (Turver 1978, 1986). Initially it was a two parameter model for predicting the radiometric temperature of an object as a function of air temperature (T) and short wave solar flux (S). This model has since been extended to the current five parameter version, to incorporate windspeed (V), cloud cover (C), and a constant to account for the temperature depression of vegetated surfaces (D). The relationship is described by;

$$R(t) = T(t\text{-}x) + kS(t) + wV(t) + C(sky,t) + D \qquad [2.4]$$

13

where R(t) is the radiometric temperature,

x is a time lag,

k and w are constants.

C, the cloud cover constant is only defined when the sun is below the horizon, as during the day it is incorporated into the short-wave solar flux, At night, C is defined by equations 2.5.

$$C(sky,t) = (20.0 - T_c) / 50.0 \qquad T_c \leqslant 0.0°C$$
$$= 0.0 \qquad T_c > 0.0°C \qquad [2.5]$$

where T_c is the sky temperature as recorded by the radiation thermometers. It is averaged over the total number of sky measurements in each scan. The accuracy of the method is increased as the amount of sky measured increases. Clear skies are associated with low sky temperatures. From this it can be seen that C increases as cloud cover decreases. The maximum value of C is therefore limited by the minimum temperature measured by the thermometer.

The time lag term, x, is incorporated into equation 2.4 to represent the thermal inertia of the material, in that the object will have a radiative temperature influenced by the air temperature at some time in the past.

An empirical model such as this requires significant amounts of data to establish it, for a wide range of objects, meteorological conditions and seasons, in order to be able to make general predictions about the behaviour of an object under a particular set of circumstances. By using linear regression techniques, the coefficients for the best-fit representation of equation 2.4 to the recorded data are calculated. The coefficients derived predict temperatures within 2°C of those actually observed.

14

Errors increase when using coefficients calculated from one period of meteorological data to predict for another period of rather different meteorological conditions; careful matching of weather conditions can minimize these differences.

Extended observations were made in 1989 in Colchester, to acquire data for a wide variety of simple plane surfaces such as grass and asphalt. Analysis of these data (McComb, Roberts, Turver 1991) demonstrated the following points concerning the model:-

• the representation of the measured radiometric data was very accurate. Deviation was typically less than 1°C, and very rarely greater than 2°C. This indicates that the five parameter model includes all of the terms that have a significant influence on radiometric temperature.

• the model demonstrates a high degree of success in predicting the radiation temperatures of objects using parameter coefficients determined from data from a few days removed from the epoch in question. Failings of the model were noted for particular objects. It is possible that this was due to the thermal inertia of the material, since the problems are associated with times when there was a rapid change in object temperature.

• the use of a set of parameter coefficients for an epoch significantly removed from that in which they were derived shows that there is still a reasonable prediction of the temperature in cases where the meteorological conditions in the two periods are similar.

2.4 Data Acquisition Equipment

The systems used to acquire the data for validating all three Durham models were developed at Durham University, using commercially available radiation thermometers.

Radiometric data were originally acquired using a Barnes PRT5 radiation thermometer, mounted on a simple computer driven platform. The system was developed continuously until 1991, when a major refurbishment and upgrade was undertaken. Descriptions of the facilities available before and after this refurbishment are included in chapter 3.

Meteorological data were gathered using one of two weather stations. For full trials, a stand-alone model was deployed, but for routine operations, one of the radiometers had the facility to connect to a weather station, and log the relevant meteorological data in the same datastream as the radiometric data from the thermometer.

2.5 Summary

Both Durham models have been successfully validated for emission from simple plane surfaces, such as grass and asphalt. The application of the Empirical Model may be extended to more complex surfaces such as layered textile materials. An investigation into the success of the of model in describing such surfaces is described in chapter 4. A large database of radiometric and meteorological information exists to allow for the validation of further developments to these models.

Chapter 3: An Improved Pointing Radiometer

3.1 Introduction

The development and validation of the models described in chapter 2 requires the availability of a large amount of meteorological and radiometric data for a wide range of natural and man-made objects under a variety of weather conditions at different locations. These data were acquired using radiometer systems designed and built in the Physics Department at Durham University. By 1991, each of these consisted of a computer-controlled platform carrying a video camera and a Medium-Wavelength Infrared (MWIR - $8\mu m > \lambda > 14\mu m$) radiation thermometer. The system had been successfully deployed on a number of experiments over a 10 year period. After the most recent of these, two of the units were significantly refurbished, following development of the improvements made on a prototype system in Durham.

In this chapter, the refurbishment of the radiometer systems is described, and the new capabilities of the units are discussed. The most recent, and detailed, calibration of the sensors is also described.

Figure 3.1 overleaf is an illustration of the refurbished radiometer system.

3.2 The Original Radiometers

The radiometers were originally designed with an observing capability in the MWIR region of the electromagnetic spectrum. This corresponds to an 'atmospheric-window', in which transmission of infrared radiation is virtually unaffected by the presence of water vapour and carbon dioxide in the atmosphere.

The capability of measuring radiative temperatures in this region was originally provided by Heimann KT17 infrared thermometers.
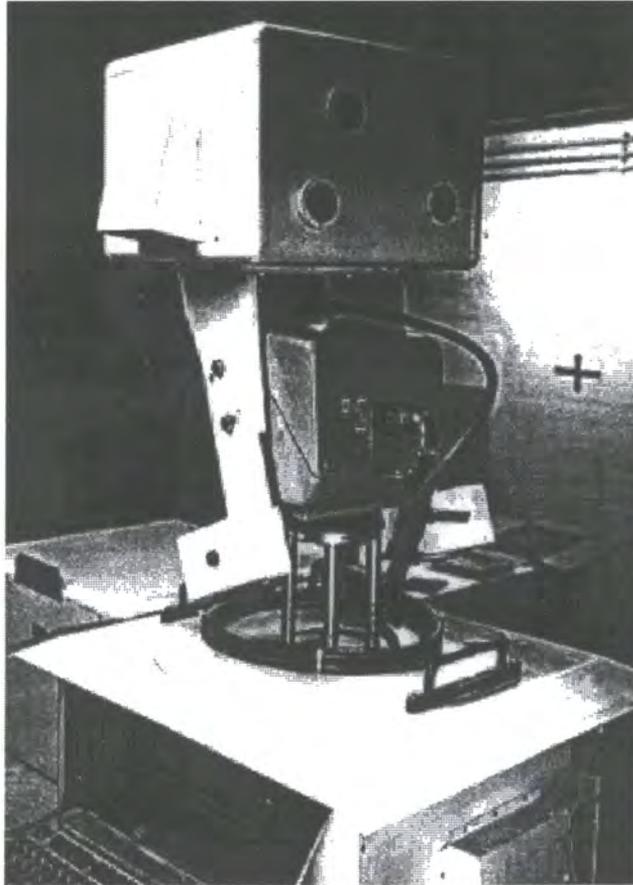
Figure 3.1 An upgraded radiometer unit, showing instrument box, pan-and-tilt head and computer box

The radiometers and a bore-sighted video camera were mounted in an instrument package which was attached to a pan-and-tilt head to point the instruments at various objects. Pointing and data logging were carried out using an Archimedes310 RISC computer. Typically, the system would be programmed to carry out measurements of around 30 objects at 15 minute intervals.

3.3 The New Radiometers

In 1992, enhancements were proposed to the specification of the radiometers. A measurement capability in a second waveband ($3\mu m > \lambda > 5\mu m$) and an improved low temperature capability in the $8\mu m$-$14\mu m$ waveband, for more accurate measurements of cloud cover were specified. These improvements necessitated the re-design of the instrument package and the incorporation of a new, heavy-duty pan-tilt head pointing mechanism.

3.3.1 The New MWIR Radiation Thermometer

The MWIR measurement capability of the refurbished systems is provided by the Heimann KT19.82 model infrared thermometer. This is the successor of the KT17 model, packaged in a more 'user-friendly' form. The relative spectral sensitivities of the two thermometers are shown in figures 3.2a and 3.2b. The data from these figures should not be used for comparison of the relative sensitivities of the two units at any given wavelength, but rather to demonstrate that the KT19 is sensitive over a wider wavelength range. The relative sensitivity of the KT19 model decays with wavelength much slower than for the KT17 model, which demonstrates a significant loss of sensitivity at $\lambda = 10\mu m$; the newer thermometer shows a broadly constant sensitivity for wavelengths up to $\lambda = 12\mu m$.
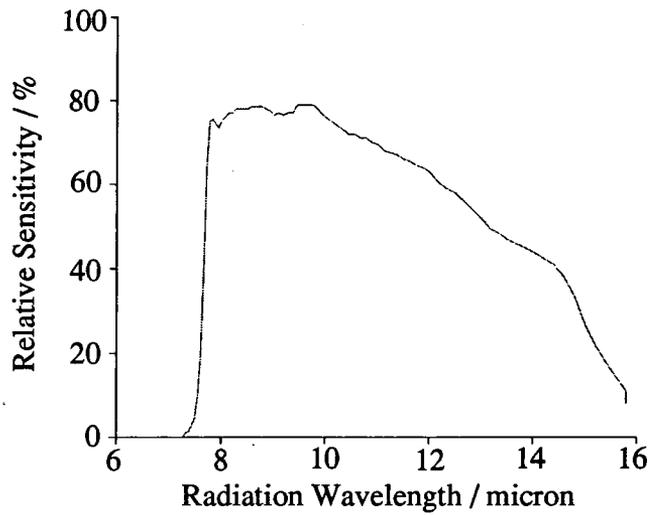
Figure 3.2a Spectral Sensitivity of KT17 Radiometer

Radiation Wavelength / micron
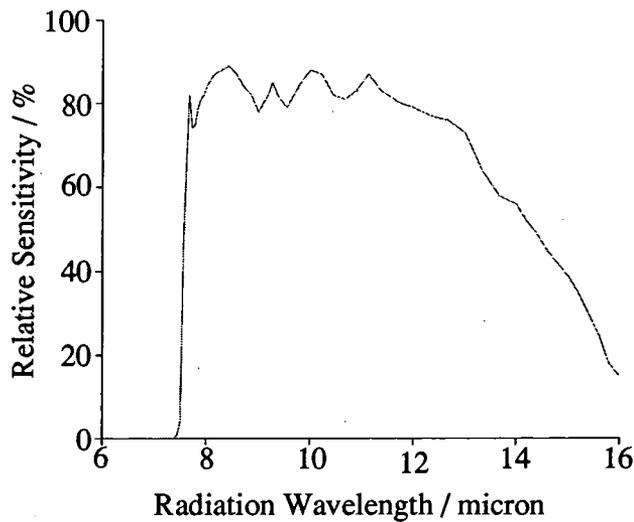
Figure 3.2b Spectral Sensitivity of KT19 Radiometer

3.3.1.1 Specifications

The KT19.82 is a general purpose MWIR thermometer. The units are supplied with a temperature measurement range definable within the limits -50°C...1000°C, with the option of a -75°C low-end capability. The KT19 incorporated into the prototype unit was to this low temperature specification, as were the thermometers ordered for the refurbished units. The output from these units is a 0...1V DC

analogue voltage, corresponding to the user defined temperature maximum and minimum of, in the prototype unit -75°C and +100°C. This allows for a temperature resolution of :-

$$R = 1000 / (100+75) \text{ mV/°C} = 5.7 \text{mV/°C} \qquad \{3.1\}$$

Therefore, a 2mV change, of the order of the noise of the voltage measurement system, corresponds to a change of 0.35°C. This is, therefore, the minimum accuracy to which any result can be quoted. Further processing of the signal in the KT19 unit results in the quoted accuracy for the temperature measurement of ±0.5°C.

3.3.1.2 Field-of-View

A knowledge of the field-of-view of an instrument is essential to the correct interpretation of data recorded. The greater the fraction of the detector field-of-view occupied by an object, the more significant will be the influence of the object on the detector output. A 2° field was specified for the thermometers used in all Durham-built radiometers. The fulfilment of the specification was verified in Durham during the commissioning of the refurbished units.
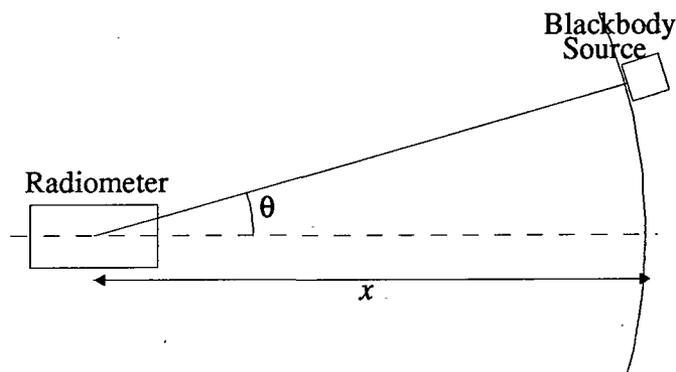
Fig. 3.3 Experimental set-up for determination of
sensor field-of-view

The field-of-view of the sensor was measured using a blackbody source, which was kept at a fixed distance from the sensor. The sensor output was measured as a function of the angle between sensor axis and blackbody, as shown in figure 3.3. A background reading was present, and was subtracted from all measurements. The field-of-view is given by a Full-Width-Half-Maximum (FWHM) definition, being the angular spread over which the signal strength is half-maximum. This method gives a representation of the field-of-view along some given axis of the thermometer. Figures 3.4a and 3.4b demonstrate measurements of the FWHM as the radiometer traverses a blackbody target along the azimuthal and zenithal axes.
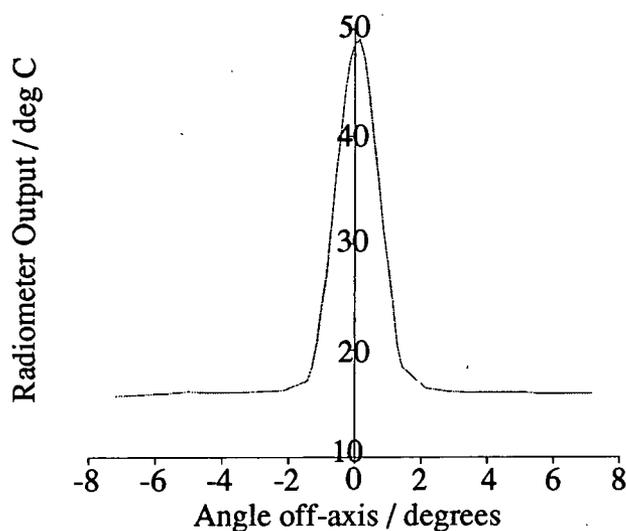
Fig 3.4a Azimuth Angle Point-Spread Function for KT19 Radiometer
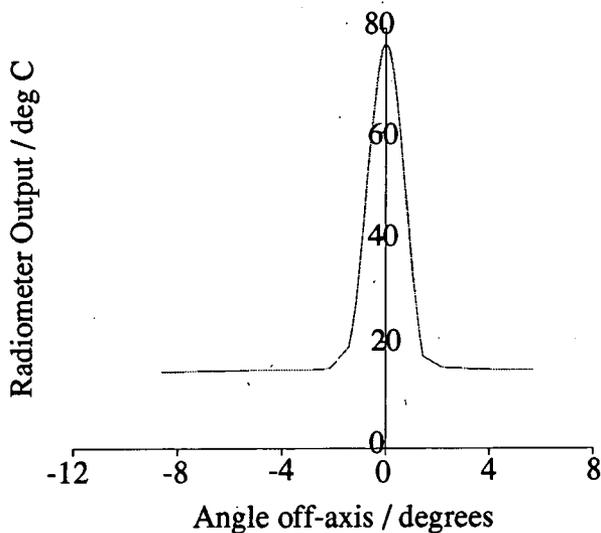
Fig 3.4b Zenith Angle Point-Spread Function for KT19 Radiometer

Measurements were carried out over a 15 metre range, corresponding to an arc of some 3.5 metres length. Full-Width-Half-Maximum measurements of the data indicate that the field-of-view of the KT19 radiometer is approximately 1.4±0.1° in azimuth and 1.6±0.1° in zenith. These readings suggest that the field-of-view of the instrument is the same along both axes, and it is therefore reasonable to assume that the instrument has a circular field of this dimension. These values indicate that the FWHM field describes a circle of diameter approximately 25 cm at a range of 10 m.

3.3.1.3 Calibration of the KT19 Thermometer

A calibration equation relating the output voltage of the KT19 radiometer to the radiative temperature is required. To determine this relationship, a blackbody source was again used. On this occasion, the radiometer and blackbody were positioned in close proximity, to ensure that the source occupied the whole of the field-of-view, so minimizing background effects. The full dataset is reproduced in Appendix A, and is summarized in figures 3.5 and 3.6. The figures show calibration data for the low-temperature modified unit, as installed in the prototype radiometer (fig. 3.5), and the standard-range thermometers, as fitted in the two other units (fig. 3.6).

Two factors were identified as having potentially significant effects on the output voltage from the thermometer, the radiative energy from the surface (directly related to its temperature), and the ambient temperature in which the thermometer is operating. Unfortunately, it proved impossible to maintain a constant ambient temperature throughout a series of measurements. However, as will be demonstrated later, the effect of ambient temperature on the thermometer output has been shown to be not large, and a change in ambient of a few degrees, as experienced during the calibrations, has negligible effects.

23

Two methods of producing a calibration equation are available. If the output of the unit is not a smooth function of the input, then the measured data points should be joined by a series of straight lines, and intermediate values calculated by linear interpolation. Thus a series of equations are produced, each valid over only a small range of input values. Alternatively, where the data points do describe a simple function, this function may be used as the calibration equation. The latter method is used here, as the relationship between input and output is essentially linear. Figure 3.5 shows output voltage as a function of blackbody temperature for the low temperature range KT19. During this calibration procedure, the ambient temperature varied from 20.7°C to 20.8°C.
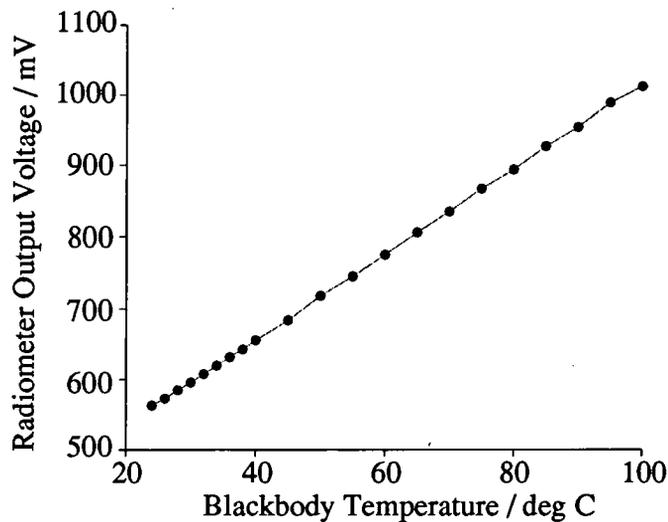
Fig. 3.5. Calibration Curve for Low Temperature Range KT19

The data are fitted by the following linear equation;

$$V = 417 + 5.98t \qquad [3.2]$$

where t is the blackbody temperature in degrees Celsius,

and V is the output voltage of the radiometer in mV.

This equation suggests a zero volts output at a temperature of ~70°C, and a maximal (~1000mV) output for a temperature of ~97°C. Both of these figures are in agreement with the manufacturers' specifications and the configuration set on the radiometer controls.

24

Figure 3.6 shows the calibration curve for the standard-range KT19 thermometer. The ambient temperature range for this set of measurements was 22.9±0.2°C.
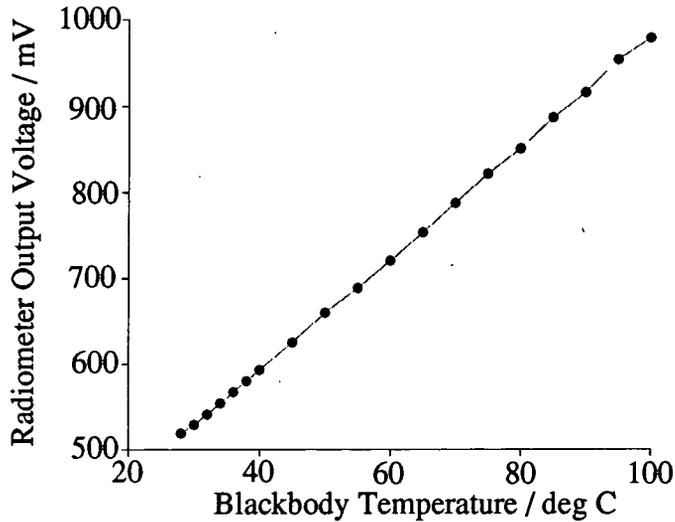
Fig 3.6. Calibration Curve for Standard KT19 Thermometer

This dataset is fitted by the linear equation;

$$V = 334 + 6.48t \qquad [3.3]$$

where V is the radiometer output voltage in millivolts,

and t is the blackbody temperature in °C.

This corresponds to a range with minimum and maximum temperatures of -51°C and 102°C respectively.

The dependence of the measured temperature on the ambient temperature is shown in figure 3.7. Within the accuracy of the instruments used, this variation can be neglected.
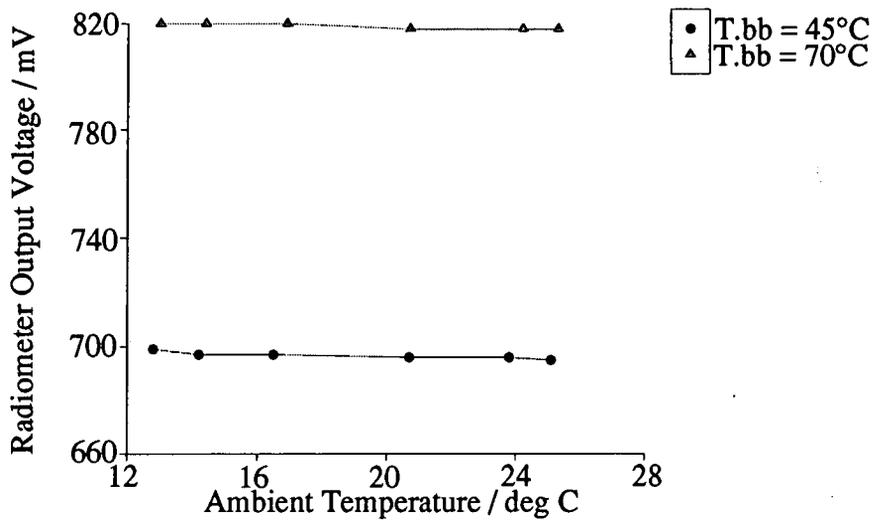
Fig. 3.7. Dependence of Output Voltage on Ambient Temperature for low temp KT19

3.3.2 The New SWIR Radiation Thermometer

Prior to the upgrade of the radiometers, the prototype system was modified to incorporate an obsolete Barnes PRT5 radiometer, operating in the 3-5μm wavelength region. This instrument is now over 25 years old, and merely served to prove the viability of the concept. For the two subsequently refurbished units, new model CE825 units were manufactured by Celect Electronics. The commissioning of these units is described below.

3.3.2.1 Specifications

The CE825 radiation thermometer is responsive in the 2-5μm wavelength region of the electromagnetic spectrum. It operates over a temperature range of 0-50°C, also corresponding to an analogue ouput voltage in the range 0-1V. The manufacturer specifies an absolute accuracy for the temperature of ±0.25°C, with a temperature resolution smaller than 0.1°C. The instrument has a response time of 5 seconds to produce an accurate output signal. Measurements made during

commissioning suggest that a response time of around 15 seconds is more appropriate if accurate measurements are to be obtained.

3.3.2.2 Commissioning the CE825 Radiometers

In order that the CE825 thermometers could be incorporated into the radiometer units, the commissioning procedure involved the determination of the field-of-view and a calibration curve for the instrument. The process used was the same as that described for the KT19 thermometers and described above.

3.3.2.3 Field-of-View

The requirement was again for an instrument with a nominal 2° field. The results of the measurement are shown in figure 3.8 below, and yield a FWHM field-of-view of approximately 2.2°±0.1°. This corresponds to a 40cm diameter target at a range of 10 m.
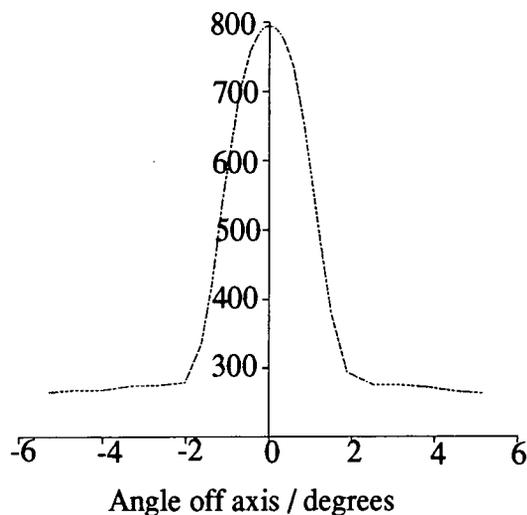
Fig.3.8. Azimuthal Angle Point-Spread Function for CE825

3.3.2.4 Calibration of the CE825 Radiometers

The calibration data for the Celect CE825 thermometers are detailed in Appendix A. Figure 3.9 shows the relationship between thermometer output voltage and blackbody temperature for an ambient temperature of 24.0±0.1°C.
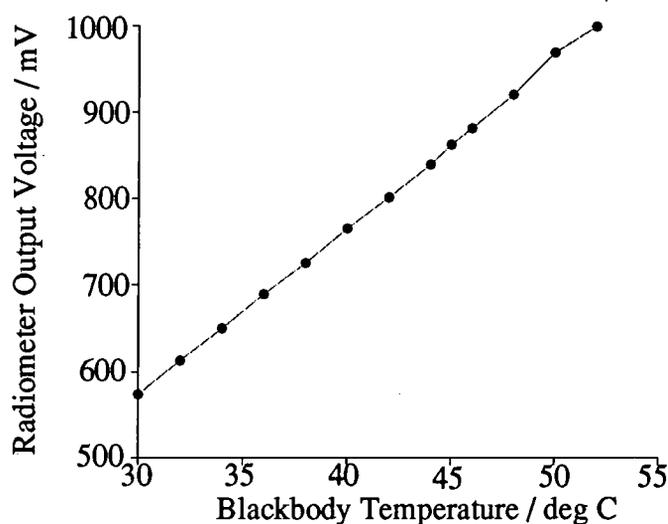
Fig. 3.9. Calibration Curve for CE825

From the graph, a certain amount of non-linearity is evident for object temperatures around 50°C, but this may be expected at the limit of the range. The linear best fit to the data is provided by the line:

$$V = -10.5 + 19.4t \qquad [3.4]$$

where V is the radiometer output voltage in millivolts,

and t is the blackbody temperature in °C.

This yields maximum and minimum measureable temperatures of 52°C and -0.5°C for the CE825 radiometer. The specification for a unit with 0°C to 50°C capability is therefore satisfied.

28

The recorded temperature measured by the CE825 radiometer demonstrates a stronger dependence on ambient temperature than is the case for the KT19 radiometer. Comparison of the datasets for measurements taken with the CE825 at ambient temperatures between 19°C and 27°C indicate a change in output voltage of the order of 1mV per °C change in ambient temperature over this range. Therefore, when used under most meteorological conditions, the effect on measured temperature of changes in the ambient temperature will be negligible.

3.3.2.5 `Warm-Up' time for the CE825 Radiometers

As with the KT19 thermometer, the output voltage from the CE825 is based on the measured temperature difference between the object being observed, and a reference temperature. This is the temperature of a metal block inside the CE825 unit, which is maintained at a known temperature. When power is first supplied to the unit, this block is not at its correct operational temperature, so initially the reference temperature is inaccurate, and all temperature measurements made will be too high until the thermometer reaches its operating temperature. An investigation of the timescale over which the radiometer reaches its operating temperature has
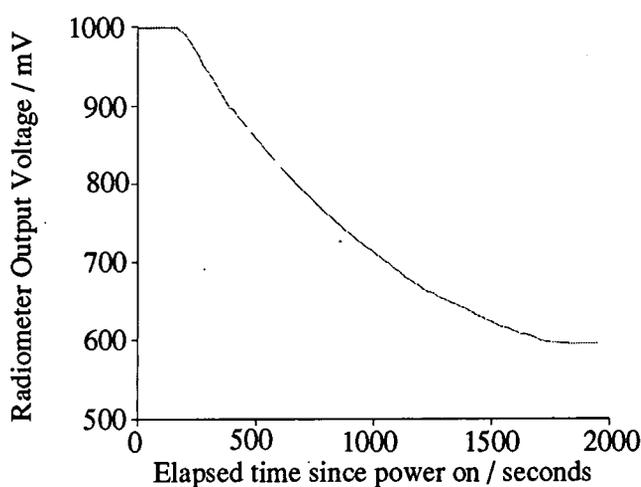
Figure 3.10. Radiometer Output Voltage as function of operating time
for model CE825 observing blackbody source at constant 30°C.

29

been undertaken. As shown in figure 3.10, this warm-up time is approximately 30 minutes, at which time an ambient temperature of 30°C was reached.

3.3.2.6 Reliability of the Radiometers

The KT17 radiometers have operated continuously for several years without problems. For a period of several weeks during the commissioning process in both bench trials and *in situ* in the radiometer units the KT19 radiometer has been fully serviceable.

The CE825 radiometers exhibited a tendency to `lock-out' at a constant output voltage on power up. This was usually cured by removing and then restoring the power supply. However, on a number of occasions this remedy proved insufficient. It appears that the model CE825 radiometer may be sensitive to either motion in the instrument box, causing failures when the radiometers were installed in the instrument packages and deployed, or that the input voltage supply is not sufficiently stable, when compared to the supply used in bench tests.

3.4 Further Modifications to the Verification Equipment

Two further significant modifications were made to the refurbished units.

The instrument packages included a bore-sighted CCTV camera to assist in aiming the radiometers. Improved CCD cameras were included in the refurbished systems to extend the dynamic range of lighting under which the CCTV camera could be used. The new cameras were provided with light-sensitive auto-irising lenses which also protect the CCDs from damage should the radiometer be pointed at the sun.

The new instrument package was significantly heavier than its predecessor, and a new platform was required to support it. Whereas the original units had side-slung pan-and-tilt heads, the refurbished units employed an up-and-over design to reduce the strain on the head caused by the increased weight.

3.5 Summary

The refurbished radiometers provide infrared measuring capabilities in the 2 μm to 5 μm and 8 μm to 14 μm wavebands, as well as an improved video record of surfaces observed.

The following calibration equations were obtained for the thermometers used.

i - Low temperature sensitive KT19 thermometer

$$V = 417 + 5.98t$$

ii - Standard-range KT19 thermometer

$$V = 334 + 6.48t$$

iii - CE825 thermometer

$$V = -10.5 + 19.4t$$

In each case, V is the thermometer output voltage (mV), and t is the temperature (K) of the blackbody target, occupying the whole field-of-view of the thermometer.

Chapter 4. An Empirical Model of Emission from Layered Surfaces

4.1 Introduction

The Durham Empirical Model dates from 1978. It predicts the thermal behaviour of surfaces on the basis of a study of previously measured temperatures and meteorological conditions, and not basic physical principles. Development of the model involves the acquisition of a large amount of field data, using systems such as those described in chapter 3. Over the fifteen years since the model was first proposed, numerous experiments have been undertaken at a variety of locations, providing measurements for a wide range of surfaces. These have provided data to develop the model, and then to establish it by comparison of its predictions with other separate radiometric measurements. Of these experiments, two of the most significant took place from September 1988 to November 1989 at Colchester, Essex and during Summer 1991, at Ouston, Northumberland. The Colchester experiment provided a significant database of measurements of thermal emissions from simple surfaces. The experiment at Ouston is the subject of this chapter.

The early experiments concerned with validation of the model dealt with simple surfaces. The use of such a restricted dataset limits the range of circumstances under which the model has been successfully tested. A logical progression from simple plane surfaces is to investigate the validity of the model in representing layered surfaces, such as vegetated and textile layers. The principal aim of this work is to investigate the ability of an empirical model to describe and predict the behaviour of complex emitters, rather than to study the characteristics of the actual emissions from the surfaces. The introduction of more complex surface combinations as typified by the textile layers allows the model to be tested more thoroughly, and any shortcomings to be identified.

The Ouston experiment, to be referred to as `Ouston II', while shorter in length than the Colchester experiment, involved a deployment of greater resources, using six radiometer units, as opposed to the two deployed at Colchester. The aim of this chapter is a description of the Ouston II experiment, and an investigation of the ability of the Empirical Model to represent the thermal behaviour of different textile layers.

4.2 The Durham Empirical Model

The model is derived from the original developed by Turver (1978,1986), which had as input parameters only air temperature (T) and short wave solar flux (S). The model has been extended to incorporate five parameters, including wind speed (V), cloud cover (C) and a constant to account for the depression of temperatures of vegetated surfaces (G). The resulting equation for the predicted radiometric temperature R(t) is:-

$$R(t) = T(t-x) + kS(t) + wV(t) + C(sky,t) + G \qquad [5.1]$$

where t is time, x is some time lag, and k and w are constants. The model has been described in detail in chapter 2.

4.3 Measurements of Radiometric Data for Textile Layers

4.3.1 The Aims of the Measurements

The aim of the experiment was to investigate the success of the empirical model in modelling the thermal responses of textile layers under a number of different conditions.

33

A variety of different textiles were used in the experiment, as described in table 4.1. The primary purpose of the experiment was not to compare the characteristics of the different materials, but rather to use the materials to provide a range of challenges for the model.

Specimen	Layer Albedo	Layer Coverage	Material
A/AII	0.294	67.5%	Polyurethane coated nylon
B	0.440	75%	Acrylic coated nylon
C	0.314	63%	Polyurethane coated nylon
D	Not known	Not known	Not known

Layer Albedo — Short Wave Albedo
Layer Coverage — Fraction of underlying surface covered

Table 4.1 Textile Characteristics

Observations of a number of textile surfaces by an individual radiometer allow a comparison of the thermal properties of the materials used, and the success with which the empirical model represents the recorded data.

Each textile was supported so that it presented to the radiometers both horizontal and inclined surfaces, so that qualitative effects of surface inclination could be investigated.

Data were collected over a period of 47 days from July to September 1991. This period included a wide range of meteorological conditions. Experience suggests that the empirical model is strongest when predicting temperatures during stable weather conditions. Selection of data from shorter periods within the trial, by careful analysis of the meteorological log, meant that this hypothesis could be investigated.

4.3.2 The Site for the Experiment

The experiment was carried out on a disused airfield at Ouston, Northumberland (lat. 55°1'N long. 1°35'W). Four radiometer systems were used to acquire data on various layered materials and numerous natural/permanent surfaces. Three of these radiometer systems were of identical construction. Data recorded by the fourth radiometer are beyond the scope of this thesis.

The observations were made close to a disused airfield runway, with large areas of tarmac and grass, which was therefore ideal for the purposes of the trial. Within the site, a number of layered textiles were deployed, over both tarmac and grass surfaces. The materials were supported so as to have both horizontal and inclined surfaces, allowing measurement of the effect of viewing angle on the measured radiometric temperatures.

The range of textiles used provided a significant challenge to the empirical model. A number of different materials were used, covering different fractional areas of the surface on which they were mounted, resulting in many layered textile/surface combinations.
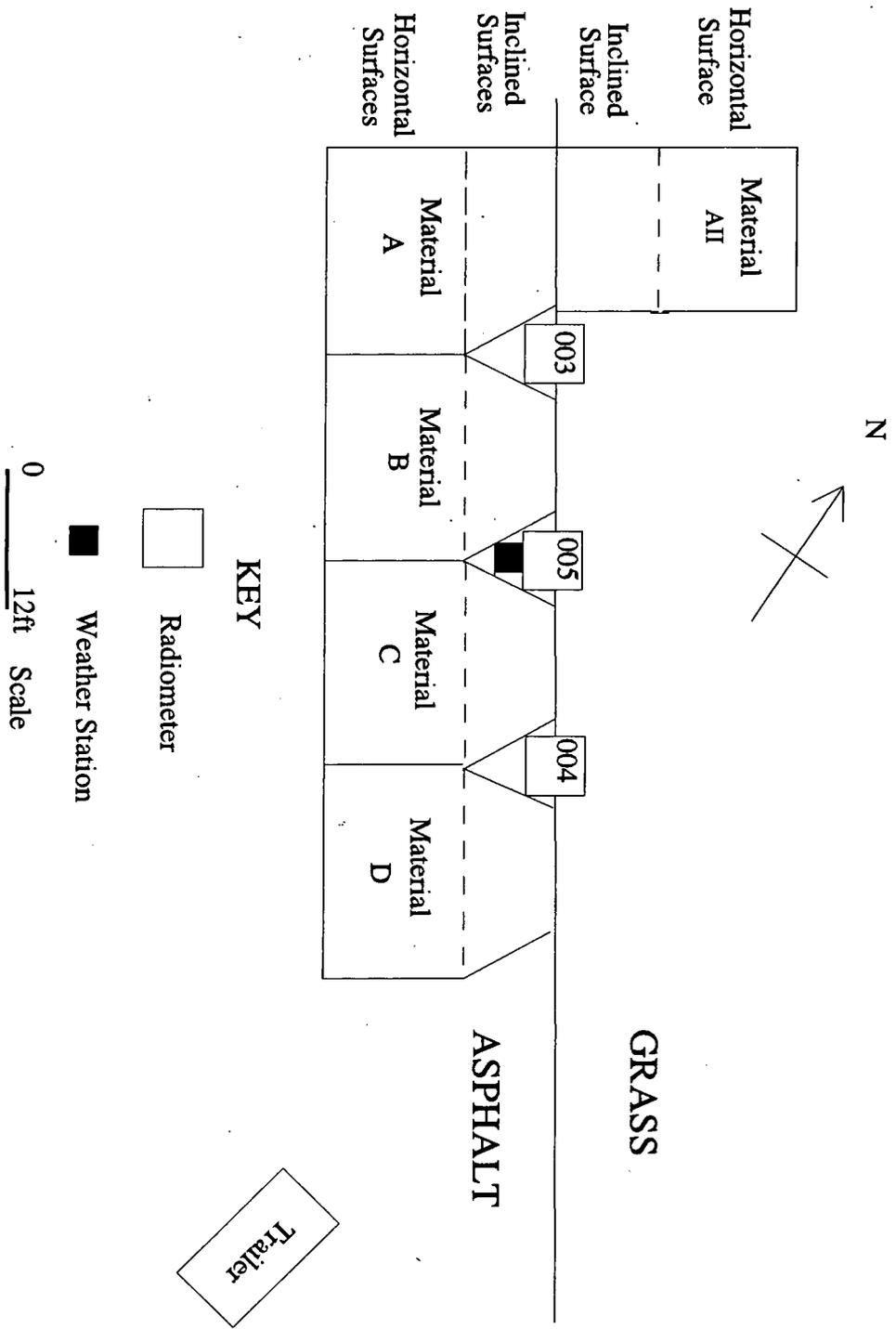
Fig.4.1. Site layout for Ouston-II trials

The layout of the site is as shown in figure 4.1. For the sections of textile shown as inclined, the slope runs from ground level at the grass-tarmac boundary, to a height of approximately 1m. The horizontal surfaces were supported at this height above the ground.

4.3.3 Description of Operational Programme

The data acquisition was carried out using three Durham-built radiometers, of the type described in chapter 3. These radiometers consist of staring radiation thermometers in steerable head units. The control systems were programmable with the azimuth and zenith coordinates of the pan-and-tilt head for pointing at a succession of objects. A typical scan would consist of between 18 and 20 object measurements, plus sky temperature recordings. Scans were made at quarter-hourly intervals. A description of some of the objects measured and more detailed results from the empirical model are shown in Appendix B.

Object materials included a range of textiles forming fractional layers over the surface, ie. the textile surfaces were incomplete, and the ground was visible through gaps in the material. The materials used were characterized by surface albedo, material construction and density of surface cover. Each material was arranged so that it presented two surfaces to the radiometers, one horizontal and the other inclined away from the ground. The site layout is shown in figure 4.1. The textiles were arranged such that the angle of inclination of the sloping surface was 45° in the centre of the material, where the radiometers were set to point. Due to the sag at the centre of the material, where unsupported, the angle of inclination at the centre of the material was greater than for the material as a whole, which had an average angle of inclination of only approximately 30°.

4.3.4 Dates of the Experiment

The experiment was carried out from July 31st, 1991 to September 15th, 1991 (Day 212-Day 258).

4.3.5 Meteorological Log

A portable weather station was used for the acquisition of meteorological data. Air temperature, incident solar radiation and windspeed were measured for the purposes of providing input parameters for the model. Radiometric measurements of sky temperatures were also taken to allow estimates of the cloud cover. The following quantities were also recorded; net radiation at surface, wet bulb temperature, humidity, surface wetness, wind direction and rainfall, although these are not at present incorporated into the empirical model. The measurement of rainfall in particular is useful in eliminating periods of unsettled weather from the dataset and explaining some apparent anomalies in the data.

Identification of Datasets for Analysis

It is impractical to investigate all measured temperatures for all surfaces for each day during the trial, so periods of representative data were selected and analysed. Each radiometer was inoperative at some point in the trial, so the suitable periods of data for study were chosen from those periods when most or all of the detectors were operational. As in previous studies, evaluation has involved identifying a period of relatively stable, fair weather, and a period of more mixed weather. This allows comparison of the relative success of the model in representing temperatures under stable and under more complex and variable meteorological conditions.

Four principal criteria are employed to determine what constitutes a period of settled weather. Since solar radiation is the main driving force behind the thermal processes involved, this is the primary concern. A smooth bell-shaped diurnal solar radiation curve is desirable, indicating that the influence of the sun was constantly present, or in the case of a very flat curve, consistently attenuated. Days with a significant amount of rainfall should also be avoided, as should periods of high windspeed, since both tend to be short term conditions and extremely variable, and so cannot be truly regarded as settled weather. Finally, extreme humidity readings are undesirable, since this parameter is not currently incorporated into the model, and its effects are unclear.

Using the criteria outlined above, two periods were identified as particularly suitable for analysis; days 241-250 (August 29th - September 7th) as a period of good settled weather, and days 235-239 (August 23rd - August 27th) as an equally settled but more overcast period. Brief descriptions of the weather for each day in these periods are given in Appendix B.

4.4 Thermal Behaviour of Layered Textiles

Radiometric temperatures for a number of textile sheets were recorded by the radiometers, in addition to a selection of simple surfaces such as horizontal grass and tarmac. Four different textiles were used, in order to provide a variety of challenges to the model. All temperature measurements were made by at least two of the radiometers, to provide redundancy and to allow cross-calibration of the radiometers. Examination of these data indicates that, in general, data recorded by different radiometers were consistent with one another, but there were examples, during both

weather periods, where the consistency is somewhat tenuous. Under some circumstances, temperatures recorded by different radiometers of the same target showed differences of up to 2°C. However, significant discrepancies are uncommon, and are not repeated systematically for different targets observed by the same radiometers. This suggests that the differences may possibly be attributed to effects due to the target, such as thermal non-uniformity across its area, as opposed to significant differences between the radiometers themselves.

4.4.1 Raw Data

4.4.1.1 Excellent Weather Period

Data recorded by different radiometers for any given surface are generally consistent with each other. For example, all radiometers recorded similar temperature variations during observations of material 'C', within a range of approximately 10°C to 25°C throughout the period. Small differences are evident in particular cases. For example, for the inclined surface, the results from radiometer 4 appear to have higher peak temperatures, by a couple of degrees, than those from radiometers 3 and 5.

Similar observations can be made for other objects observed by all three radiometers. For example, the horizontal surface of material 'B' has a measured minimum temperature from radiometer 5 during the night hours of days 241/242 about 2°C lower than that measured by the other two radiometers.

The agreement between measured temperatures for different radiometers for the permanent surfaces (tarmac, grass) is generally better than for the textile surfaces. Possible reasons for this, and for the discrepancies noted above, are discussed later.

4.4.1.2 Mixed Weather Period

Once again, the temperatures recorded by the different radiometers are generally in agreement with one another, with a few cases where the agreement is not particularly close. For example, the midday peak temperature for day 237 for material 'C' as measured by radiometer 4 is significantly higher than the temperature recorded for the same object by the other radiometers, but once again the temperatures of the tarmac/grass surfaces exhibit a higher degree of uniformity than is the case for the textiles.

Permanent surfaces such as tarmac and grass have high spatial uniformity compared to the lighter material surfaces. As shown in figure 4.1, large areas of grass and tarmac were available for observation. This reduces any ambiguity due to small pointing errors, as it is always possible to select a radiometer position such that the field-of-view is entirely occupied by the surface, whereas this may not always be the case for the textile surfaces.

There are a number of possible reasons why two different radiometers should record different temperatures for the same object. The different viewing positions of two radiometers relative to a surface mean that the object may occupy different fractions of the fields-of-view of the two radiometers, and the background temperature effects may therefore be different. This effect is related to the zenith angles at which the instrument heads are pointed. Large zenith angles correspond to the radiometer looking approximately straight down onto the material, and the textile will occupy most of the field-of-view of the detector. A smaller zenith angle corresponds to the radiometer head being closer to horizontal and parallel to the material surfaces. Thus, the effective area of the material as seen by the radiometer is reduced, and the contribution of the background temperature may be increased.

41

An alternative source of potential error is the direct reflection of solar radiation from the material surface into the radiometer lens. This will be a maximum when the textile is directly between the radiometer and the sun, and a minimum when the sun is behind the detector.

It is possible that there are genuine spatial variations in temperature across a textile sheet. Where two radiometers are positioned close to a sheet, they may view different parts of the material, with differing textile coverage of the underlying surface.

4.5 The Representation of the Observed Data by the Model

The Empirical Model was used to provide a representation of surface temperatures derived from measured meteorological data. A non-linear regression utility was used to produce the best fit to the measured radiometric data. Comparisons were drawn between the measured temperatures and the model representations. The model results and the associated errors are reproduced in Appendix B.

The success of the model in representing the radiometric data in terms of the meteorological data is compared for measurements using different radiometer units; for flat and inclined surfaces of the same material; for different materials under the same weather conditions; and for identical surfaces under differing weather conditions. The comparison of data obtained with different radiometer units is made to demonstrate that all data are equally suitable for analysis.

The success of the model in representing the data in a particular set of circumstances can be gauged by the values of the mean and RMS residual errors of the model results when compared to measured data. Smaller residual errors indicate a closer representation to the measured data.

An examination of the coefficients of the parameters in the model suggests that the solar radiation is the dominant term in the model's representation of the surface radiometric temperature. Relative to this, the other terms make significantly smaller contributions. Thus, the model can be used as a tool to identify key aspects of the thermal behaviour of the surface which are due to the solar radiation.

4.5.1 Comparison of Temperatures Measured by Different Radiometers

An analysis of the residual differences between the representations of radiative temperatures by the model and observational data recorded by a range of measuring devices suggests that there is no significant difference between results recorded by different radiometers. The residual values are similar in magnitude and any differences do not show any obvious trend. For example, the residual values for observations by radiometer 5 during the good weather period appear to be consistently smaller than those for observations by radiometer 4. This tendency is not repeated for observations in the mixed weather period, when the residual values calculated for radiometer 3 measurements appear to be highest. In general however, these discrepancies are of insufficient magnitude to be deemed significant. There therefore appears to be no reason to suggest that there is any difference in the quality of data recorded by the different radiometers.

4.5.2 Comparison of the Temperatures of Horizontal and Inclined Surfaces

A comparison of the average residuals for the fits by the empirical model to the temperatures of the flat and inclined surfaces of a material suggests that the model represents the temperatures of the horizontal surfaces more accurately. In most cases, the goodness-of-fit residuals for the horizontal surfaces representations are approximately 80% of the values for the inclined surface data. An analysis of the absolute magnitudes of the coefficients in the parameterization shows no consistent trend in the dominant solar radiation term when comparing measurements of horizontal and inclined surfaces. For example, the solar radiation is more strongly coupled to the temperature of the inclined surface of material 'B', while for materials 'C' and 'D', the coupling is stronger to the temperature of the horizontal surface.

4.5.3 Comparison of Measurements of Temperatures of Different Surfaces

The empirical model successfully predicts the thermal responses of the textile layers to a level of accuracy at least comparable to that demonstrated for the asphalt/grass surfaces. The goodness-of-fit residuals for the asphalt surface measurements are up to twice the size of the values appropriate to the textile surfaces. Comparison of the residuals for textile and grass surfaces shows similar trends. There appears to be little difference in the quality of the representation of the temperatures of the different textiles by the model, with all having residuals of ~0.9°C.

Comparison of the coefficients of the parameters in the model shows that the solar radiation coefficient is smaller for the textile layers than for asphalt and grass surfaces. This suggests that temperatures of the textile layers are less dependent on solar radiation than the temperatures of the grass/asphalt surfaces. Comparison of

the model coefficients for the representation of the temperatures of the individual textiles indicates that material 'A' is the most strongly coupled to the solar radiation. Material 'B' shows the weakest coupling. This difference may be related to the different albedos of the materials. As shown in table 4.1, material 'A' has the lowest albdeo of the textiles, while that for material 'B' is nearly 50% larger.

The parameters for the air temperature coefficient in the model are generally smaller in magnitude for the representations of the textile surfaces than for the grass and asphalt. This indicates that the coupling between air temperature and textile temperature may be weaker than that between air temperature and grass/asphalt temperatures. The difference in coupling is less marked than is the case for the coupling to solar radiation. The fits to measurements of textile surface temperatures produce coefficients which are typically between 40% and 100% of those for the measurements of the temperatures of the ground surfaces.

It appears that the different textile and grass/asphalt surface temperatures exhibit no dependence on windspeed. No trend is apparent in the model windspeed coefficients for representations of the different surfaces. It also appears that there is no relationship between any surface temperature and the temperature depression.

In summary, only the coupling between surface temperature and solar radiation appears to differ between textile and asphalt/grass surfaces with high statistical significance. There does appear to be some difference in the effect of air temperature on surface temperature, with asphalt and grass being more strongly coupled to this parameter, but the difference is less significant than for the coupling to solar radiation. It is again stressed that the model does not represent the radiative temperature by calculating any physical effects. It simply provides the best representation in terms of the four parameters available, with no consideration for the

physical logic of the results it produces. As a result, the absence of any correlation between representations of the temperatures of different surfaces for two of the parameters is unsurprising. As solar radiation is regarded as the dominant effect on temperatures as represented by the model, it is the coefficient that would be expected to show a correlation.

4.5.4 Comparison of Temperature Measurements Under Different Weather Conditions

A comparison can be made of the average goodness-of-fit residuals for the representations of temperatures of the same object measured during the two weather periods. This shows that the residuals are typically smaller during the mixed weather period, which indicates that the model represents the radiometric data more accurately under mixed weather conditions. This may be a result of the absence, due to the prolonged presence of cloud-cover, of the more extreme temperature variations associated with a very high incident solar flux.

One fact of note is that, for the excellent weather period, the coupling between air temperature and surface temperature is consistently negative. This is a result of the unphysical nature of the model, and may be accounted for by the fact that the four parameters are not truly independent, and the air temperature is coupled to the solar radiation and the effect of changes in air temperature are completely obscured by the more dramatic changes in incident solar radiation.

No consistent trend emerges in a comparison of the coupling of surface temperature to solar radiation for different surfaces during the two weather periods. There are insufficient data to suggest trends in the variation of any of the other model parameters under changes in weather conditions.

4.6 Summary and Conclusions

The experiment at Ouston in 1991 was carried out with a view to investigating the validity of the Empirical Model for 'thermally light' targets such as textile layers. The results show that the temperatures predicted by the empirical model for all of the textile samples are typically within ~1°C of the measured temperatures and very rarely more than 2°C different, under both good and mixed weather conditions. There is some indication that the model appears to represent the measured data better in the mixed weather period. This is consistent with previous findings (Edwards, McComb, Turver 1993).

The results also support the observation made previously (McComb, Roberts, Turver 1991), that the performance of the model deteriorates when dealing with rapid changes in surface temperature. It fails to accurately represent the maximum temperatures reached by a surface during the middle of the day, if such temperatures are only attained for a short period of time. A similar weakness is noted for low night-time temperatures.

This analysis demonstrates the suitability of the Durham Empirical Model for representing the thermal behaviour of a variety of textile surfaces, as examples of thermally light materials, under different climatic conditions. The model was found to represent such materials with a level of accuracy comparable to that attainable for heavier targets such as asphalt and grass, as investigated previously (McComb, Roberts, Turver 1991, Edwards, McComb, Turver 1993).

The challenges set for the Empirical Model by this experiment involved accurately representing the thermal behaviour of surfaces with significantly different physical characteristics to those investigated in previous analyses. The results presented here show that the model has successfully met these challenges, and can be used to represent 'thermally light' surfaces.

Chapter 5. The Outline Of A Detection Model

5.1 Introduction

Detection models are used in a variety of applications to provide an indication of how a particular sensor system will represent a given scene under specified conditions. Examples of systems for which there is a modelling requirement include military sensors used to search for potential threats, and crop monitoring in agricultural regions, where healthy crops may have different thermal signatures from diseased or infested areas. A proven model has uses beyond being merely predictive. It can be used to demonstrate thermal signatures of significant features for future recognition and comparison, allowing active searching for specific information within a dataset, with associated savings in time and manpower.

The output from a detection model usually takes the form of a prediction of how the sensor will respond to changes in any of a number of parameters affecting the surface, atmosphere or sensor. Complete models are often modular in construction, in that these sections are treated individually as sub-models linked in series, such that the output from one sub-model forms the input parameters for the next. For example, the calculated properties for the thermal signature of an object and background form the inputs for the part of the model considering the effects of the atmosphere. This is not an unreasonable treatment for simple object-atmosphere combinations. Furthermore, these sub-models can often be divided into even smaller components, especially in the case of a sensor model, where a number of different features influence the processing of the input signal. The simplest division of the sensor model is to separate modelling the optics and electronics of the system. The treatment of the sensor may also be extended to include the observer, who can then be treated as a separate sub-model.

The components of a detection model are defined by the function of the system it is designed to simulate. Most detection models will consist primarily of the surface/background, atmospheric and sensor sub-models. How these sub-models are subsequently divided may vary. Of prime consideration is the required accuracy of the model, and the complexity of the programming required to implement it. A balance must often be struck between predictive accuracy and computational speed. The greater the required accuracy, the more detailed the sub-models must be. An example implemented in SENTRAN, (the version of the atmospheric transmission code LOWTRAN used by PC-SenSAT) is the influence of sky radiance on a surface. This variable can be computed for each cycle through the program, or just for the first cycle, with the same value used on subsequent occasions. The former is obviously more accurate, but takes significantly more time to compute. Similarly, a detection model such as SENSAT-3, which deals with radiation in the region $0.2\mu m < \lambda < 28\mu m$, must take account of the fact that, for $\lambda < 1.0\mu m$, sensor spectral response is defined by quantum efficiency $\eta(\lambda)$, while for $\lambda > 1.0\mu m$, it is defined by the detectivity, D^*. Thus, a simple model, designed for a single purpose may be relatively straightforward to implement, whereas commercial packages, intended for a wide range of problems, need to cater for a combination of possible circumstances.

Model complexity also increases with the generality of circumstances for which the model is designed. One of the most common figures-of-merit for a detector is the MRTD (Minimum Resolvable Temperature Difference). The MRTD of a particular sensor may vary little under a narrow band of conditions and may legitimately be approximated by a constant, and so a simple MRT-based model is relatively trivial. However, if it is necessary to model the response of a number of sensors, then the MRT must be calculated depending on sensor characteristics.

5.2 An Overview

Detection modelling is a post World-War-II science and much of the early work was led by military requirements. The development of optical and infrared detection systems has occured concurrently, with much of the science being common to both. Therefore, it is perhaps not surprising that much of the work on modelling sensor systems until the late 1970s was based on work done at the U.S. Army Engineer Research and Development Laboratories, on optical image forming/intensifying systems (Johnson, 1958). In this paper, Johnson reduced the imaging system to a series of 'black boxes', and dealt only with the input and output from each stage. He ultimately identified six possible output states for the intensifier, varying from no detection to object identification. For non-imaging systems, the number of outputs is somewhat reduced, with the object either being detected or not. Johnson also defined the criteria for the three levels of object observation; detection, orientation and identification. The target is treated as a series of contrasting dark and bright line pairs. Johnson showed that target detection, orientation and identification could be defined by the number of line pairs that can be resolved at the sensor. Johnson quotes examples for a number of military targets. This simple method of treating targets is defined by target/background contrast, as well as line spacing and target-sensor range. The criteria were used as the basis for a number of detection models, including the Night Vision Laboratories Static Performance Model (NVLSPM), to be detailed below.

5.3 The Target Model

For the purposes of a detection model, a target is defined as any object within the field-of-view (FOV) of the sensor. Many detection model packages predict the thermal signature of the targets within the FOV, based on the simple physical

51

properties of area, temperature and emissivity. Examples of such models include SenSAT, as described in chapter 6, and the Night Vision Laboratories model detailed in section 5.6. Target area is a constant, assuming that the target does not fill the FOV. Emissivity is a function of wavelength and aspect angle, and can be found in tables (Monteith and Unsworth, 1990). However, for most surfaces, the emissivity variation within the infrared region of the spectrum is small, and emissivity can also be regarded as constant. Surface temperature can be measured by means of a contact thermistor, which may be adequate, although this may have a disruptive effect on the target temperature. However, there are obvious occasions, when making contact measurements is impractical, such as satellite observations of large areas. In such cases, it is desirable to make predictions of the target temperatures from either basic physical principles or from a series of measurements of temperatures and the corresponding meteorological conditions. The Durham Empirical Model, as described in chapter 2, predicts the temperature of a surface on the basis of meteorological conditions. The other Durham models described make predictions based on the physical properties of the material being measured and the weather conditions.

5.4 The Model For Atmospheric Transmission - LOWTRAN

The atmosphere attenuates the strength of radiative energy passing through it by two methods; absorption and scattering. The most common model in use for the prediction of atmospheric effects is the United States Air Forces Geophysics Laboratory's LOWTRAN model.

The LOWTRAN code is complex, and for short paths between object and detector in clear atmospheres, it may be adequate to replace it with a simple exponential decay function for the signal strength with range. However, the implementation of an accurate atmospheric code is necessary for path lengths in excess of a few hundred metres.

LOWTRAN deals with molecular scattering and absorption, due to the composition of the the atmosphere, and particular scattering due to aerosols, clouds, smokes etc.. The atmosphere is defined as a series of horizontal layers. At ground level, the boundary layer is significantly affected by ground conditions, defined by the type of ground cover. Predefined datasets exist for defining rural, maritime, desert and urban conditions etc. The concentration of different gas molecules at different altitudes are specified in gas profiles. The amount of detail in these profiles defines the number of layers. Since different molecules absorb energy corresponding to radiation of different wavelengths, varying the gas profiles controls the absorbtion of specified wavelengths at given altitudes. The effects of absorption by molecules in the air is relatively small in the 8-14μm region of the electromagnetic spectrum.

Particular scattering and absorption have similar effects, and may also attenuate signals in the 'atmospheric window' where molecular effects are negligible. For this reason, it is necessary to implement an accurate atmospheric model, such as LOWTRAN, even over short object-detector ranges, where the atmosphere contains some form of smoke or obscurant, as an exponential approximation may be invalid.

LOWTRAN is a single scattering model. This means that scattering only has attenuating effects, in that radiation can only be scattered out of the path from surface to sensor. It follows that this radiation is scattered into adjacent paths, but the

original LOWTRAN code does not consider increases in signal strength due to the presence of radiation scattered from other paths. The result is that LOWTRAN may predict that the signal received by the sensor is smaller than it actually is.

The method of atmospheric layering has also been shown to cause inaccuracies in LOWTRAN calculations (Cornette, 1992), particularly near to the surface of the Earth. This is due to the fact that LOWTRAN does not consider temperature gradients within an individual layer, but relies on interpolating between the two boundary values, and that the gradient is most marked at low altitudes. This interpolation is crude, and is the cause of the problem. It is observed that the problem can be solved by subdividing the layer into a large number of thin layers, but that this trial-and-error method is impractical in many circumstances. Cornette overcomes this problem by making an approximation to the emitted radiance which involves a refined interpolation process. Results quoted indicate a reduction in maximal and r.m.s. errors of two orders of magnitude over the original code.

5.5 The Sensor Model

Sensors can be classified as one of two types, imaging or single element staring systems. Imaging systems in particular, have become significantly more complex with the introduction of new techniques. Modern sensors employ processes such as sampling and aliasing, which do not feature in first-generation systems.

Suitability of a sensor for a particular task is defined by a figure of merit. Unfortunately, no standard figure has been developed, with different approaches to the problem yielding many different figures of merit.

The simplest figure of merit is the Minimum Detectable Temperature Difference (MDTD). This is typically used for small, hot objects, describing an angle smaller than the sensor field-of-view for a non-imaging sensor, or smaller than the field-of-view of a single pixel in a staring imaging sensor. The result is that the signal is `smeared' over the pixel on which it falls, causing an increase in the output from the individual pixel. The MDT is the smallest difference in temperature between a point-source object and background that would be detected by the sensor. It is inversely dependent on pixel area, since the larger the pixel area over which the input signal is smeared, the smaller the output signal. In the limit where the signal falls exactly on the area of one pixel, the result is a maximum strength output signal. Considering a pixel twice as long on each edge, the same signal falls on only 25% of the pixel. The other 75% of the pixel detects no input signal, and the result is that the output is only one-quarter of the maximum. MDT is also dependent on background temperature, as detectors measure not temperature, but the energy emitted by the surface, which, by Stefan's Law, is proportional to the fourth power of the temperature when integrating over the full range of wavelengths, from 0 to infinity. From this premise, it is straightforward to show that the change in luminosity due to a change in surface temperature is given by, to a first order approximation;

$$\Delta L(t) \propto t^3 \qquad\qquad [5.1]$$

Perhaps the most common figure of merit is the Minimum Resolvable Temperature Difference (MRTD), introduced by Genoud and Sendall (Lloyd, 1975). Resolution is a higher order process than simple detection of an object, and involves recognition of object features. The Night Vision Laboratories Static Performance Model (NVLSPM), described below, is an MRTD-based model. MRTD also has a dependence on pixel size and background temperature, but is also affected by object range, since the object is not treated as a point source, but at least two edges of the

object are visible against the background. Thus the object's position is definable; it has been resolved from the background. Despite the popularity of this figure of merit, discrepancies remain between theoretical predictions of MRT and field performances. It has been proposed (Karim *et al*, 1991) that MRT is merely a special case of a more general Minimum Resolvable Luminance Difference (MRLD). MRLD is shown to overcome a number of the problems with temperatures predicted by MRT models. It is also suitable for graybody and spectrally selective sources, as found in nature. MRT is only applicable for blackbody sources.

Both MRT and MDT are derived by combining the Modulation Transfer Functions (MTFs) of the detector components, with the detector Noise Equivalent Temperature (NET or NEΔT). Any electronic system generates noise on the output signal. In the case of a sensor, this noise will have a magnitude corresponding to some object temperature in excess of the background, and is the NET. It therefore follows that a sensor cannot distinguish between objects at temperatures separated by less than the NET. Once again, although the noise will have a maximum amplitude, the NET to which it corresponds is also dependent on the absolute object temperature.

5.6 Combined Detection Models

5.6.1 A Static Performance Model

One of the earliest widely used detection models was developed by the United States Army. The NVLSPM was presented as a model for predicting the probabilities of the various levels of object observation as functions of object-sensor range for different thermal signatures, atmospheric conditions and system parameters (Ratches, 1976). The model is described as 'static' because no search processes are

involved. It deals with the case where the object is within the field-of-view of the sensor, and predicts the probabilities of detection, recognition and identification, based on properties of the object and its background. It has been widely used as the basis for many subsequent detection models.

This model is a good example of the modular nature of many detection models. The target sub-model is remarkably simple. The thermal signature is derived from the areas A_i, and temperatures T_i, of objects within the field of view. The target is ultimately treated as a rectangle of dimensions H x l. H is the critical dimension, usually being the smallest resolvable dimension of the target. l is then chosen to give the same emissive area as the real target. The effective average temperature of the target is an area weighted average, defined by the expression:

$$T_{AVG} = \frac{\Sigma_i A_i T_i}{\Sigma_i A_i} \qquad [5.2]$$

The target signal strength is defined from the target and background temperatures by Planck's Radiation Law as shown.

$$\Delta L = \int_{\Delta\lambda} \Delta L_\lambda \, d\lambda$$

$$= 2 c^2 h \int_{\Delta\lambda} [(\exp (h.c/\lambda.k.T_{AVG}))^{-1} - (\exp (h.c/\lambda.k.T_B))^{-1}] \, d\lambda \qquad [5.3]$$

where ΔL_λ is the spectral radiance sterance ($w.cm^{-2}.sr^{-1}.\mu m^{-1}$),

$\Delta\lambda$ is the spectral bandpass (μm),

c = velocity of light (3×10^8 m.s^{-1})

h = Planck's constant (6.6252×10^{-34} W.s^2)

k = Boltzmann's constant (1.38047×10^{-23} JK^{-1})

Multiplying ΔL_{AVG} by H.1 will give the model estimate of the total watts per steradian emitted by the target. Thus the estimate of the total radiance of the target can be passed to the atmospheric sub-model. Most detection models use commercially available atmospheric models. This one uses LOWTRAN, as described in section 5.4. As an alternative, for use in simple calculations, an exponential decay function can be used, although it is not strictly valid, particularly over long distances. In this case, the model would use the expression:

$$\tau_{\Delta\lambda}(R) = e^{-\alpha R} \qquad [5.4]$$

with τ the transmission, R the range from the target and α the attenuation coefficient representing absorption and scattering in the atmosphere. The effective temperature difference between target and background at range R is given by $\Delta T'$, as a function of ΔT (= ΔL), the effective temperature difference at the target by the relationship:

$$\Delta T' = \tau_{\Delta\lambda}(R) \cdot \Delta T \qquad [5.5]$$

The effective radiance difference at range R is therefore given by the expression:

$$\Delta L' = \tau_{\Delta\lambda}(R) \cdot \Delta L \qquad [5.6]$$

Of the many detector figures-of-merit described in section 5.5, the most suitable for a single element staring detector is MDT (Minimum Detectable Temperature Difference). Simply substituting $\Delta L'$ from equation 5.6 for ΔL in equation 5.3 will give an estimate of the radiance difference between target and background as viewed at some range R (equation 5.7).

$$\Delta L' = 2 c^2 h.\tau_{\Delta\lambda}(R).\int_{\Delta\lambda} [(\exp (h.c/\lambda.k.T_{AVG}))^{-1} - (\exp (h.c/\lambda.k.T_B))^{-1}] d\lambda \qquad [5.7]$$

If ΔL' is greater than ΔL$_{min}$, which corresponds to ΔT = MDT, then the target is detected by the sensor. Equation 5.8 is derived from the Stefan-Boltzmann law (equation 1.1).

$$\Delta L_{min} = 4\varepsilon\sigma T^3.(MDT) \quad \text{(to first order)} \tag{5.8}$$

MDT is defined by Ratches by equation 5.9. The Fourier Transforms are defined for the individual components, and a number of examples are quoted in the paper.

$$MDT (W) = (S/N)'.(NET/A_T \int H^2_W \cdot H^2_{TOT} \, d^2f) \tag{5.9}$$

where (S/N)' is the threshold signal-to-noise ratio for detection,

NET is the noise equivalent temperature,

A$_T$ is the target area in radians^2,

H are Fourier Transforms for the target and sensor/eyeball combinations.

5.6.2 Other Detection Models

The relationship between visual detection models and general optical/infrared detection models is demonstrated by the Autonetics Detection Model (Greening and Wyman, 1970). This model was developed to estimate probabilities of the various levels of target acquisition for observers in aircraft. The model takes account of the properties of target and atmosphere, but no detector is considered. Instead, the model attempts to account for the detection processes within the human brain. When representing the target, light levels must be considered, rather than temperatures, but it is the target/background contrast that is again critical to the level of detection. The model also considers the number of resolution elements (dark/bright line pairs) required to resolve critical detail, in a similar fashion to Johnson.

The Infrared Atmospherics and Signatures Prediction Model (IASPM) is another United States military development (Kreiss *et al*, 1991). It is a hybrid model, constructed from a number of well established sub-models. It is concerned with imaging sensors, and is described as being an 'end-to-end' model, meaning that it deals with all aspects of target, atmosphere and sensor. The model is valid over the 1μm to 20μm region of the electromagnetic spectrum. Developed for the United States Air Force (USAF), the model is concerned with the detection of aircraft. The target model is a combination of the USAF models SPIRITS, which models hard objects, such as the plane, and JANNAF SP1, which is a plume code, for modelling the exhaust gases. The atmospheric model incorporated is MODTRAN, which is a more sensitive version of LOWTRAN. Simulations carried out in the 3 to 5μm and 8 to 12μm regions of the spectrum clearly show a number of distinctive features, including the resolution of body areas of different temperatures. Validation data confirmed the ability of the model to identify particular types of aircraft, by comparison of measured results with wireframe models in the SPIRITS model code.

Also of note is the MICOM Infrared Imaging Systems Performance Model (MI2SPM), which is used as a basis for graduate remote sensing courses (Salvaggio *et al*, 1990). The MI2SPM is based on Ratches' NVLSPM code, but is extended to consider modern focal plane array (FPA) charge-coupled devices (CCDs). The authors describe the basic premises from which figures-of-merit are derived, and the particular applications for which each figure is suitable. The paper goes on to use the MI2SPM to compare three different detectors under a variety of conditions relating to target and atmosphere, including NET and target-background temperature difference. This highlights the features which must be taken into consideration when developing a model for a thermal infrared imaging system.

5.7 Summary

The wide variety of commercially produced detection models is a result of the many different imaging requirements for which they are created. However, all have a number of common features, in that they are modular in construction, with separate sub-models used to calculate the properties of the sensor, atmosphere and target. The advantage of this method is the ease with which one sub-model can be replaced by another to produce a model suitable for a particular set of characteristics. The figure of merit, which defines the level of performance required to achieve some level of detection is also dependent on the characteristics of the scene being modelled.

While there are a large number of target models, these can be divided into two categories; those that model solid objects and those that deal with radiative sources such as aircraft exhaust plumes.

LOWTRAN is almost an industry standard model for atmospheric transmission. Others exist (FASCODE, TABLOW), but are used much more rarely.

Sensor models are usually device specific, since sensor characteristics vary greatly between units. Device nonspecific models can serve really only as a general starting point for producing data for a particular sensor.

Chapter 6. Evaluation of a Detection Model Package

6.1 Introduction

The components of a generic Detection Model have been outlined in chapter 5. Software is available commercially which models some or all of the features described. One such package is the software suite PC-SenSAT, produced by the ONTAR Corporation, USA. This chapter describes the evaluation of this software, with a view to combining SenSAT (or a similar suite) with the Durham General Purpose Model (DGPM) and a graphical display package, to produce a combined detection model.

SenSAT is designed to simulate systems operating within the spectral waveband 0.2μm-28.5μm. The basic purpose of the software is to calculate the signal output from a detector as a function of a number of independent variables relating to many of the properties of the object, atmosphere and detector. Potential uses of SenSAT include optimizing the characteristics of a sensor for particular circumstances, and investigating the effects on detection of changes in the composition of the atmosphere.

Hardware and Software Requirements

The software evaluated is an enhanced version of the SenSAT package, designed to take advantage of the capabilities of an 80386-based PC with a minimum of 2Mb of extended memory. A minimum of 3Mb of hard disk space is required, and an 80387 maths coprocessor is desirable. 525kb of Conventional memory is also required. Since current PCs (IBM compatible Personal Computers) have only 640kb

of Conventional memory in total, this is a significant limitation. The principal advantage of the enhanced version is one of computational speed, but it also allows for the calculation of more detailed results.

6.2 The SenSAT Package

6.2.1 Software Construction

Software versatility was a high priority in the design of the SenSAT package. The surfaces, atmosphere and detector are treated separately, and predefined options are included for the most common values of many of the variables. For example, the spectral response functions of twenty-four sensors are included, ranging from theoretically ideal units to representations of commercially available detectors. However, there is also the facility to define a sensor response curve, should none of the options prove suitable.

A range of outputs from the suite are available. The option of most interest produces plots of detector response to variation of some independent variable. The output is expressed as a number of response-related variables (Signal-to-Noise Ratio (SNR), Brightness Temperature, Radiance) as functions of the variable. Other options include displaying the relative response of the detector as a function of wavelength and a spectral band optimization. For this option, detector response is plotted as a function of both spectral band width and band centre, resulting in a 3-D surface plot. This provides an indication of the frequency range over which a signal is strongest, allowing the most suitable detector to be chosen for a particular application.

When using the standard option of measuring output signal strength as a function of some independent variable, two such variables may be selected, but instead of producing a 3-D surface plot, the second is treated as a parameter, and a separate curve is plotted for each value. The variables may be chosen from the following:

Wavelength (for band optimization plots only)	Altitude
Observer (detector) altitude	Target altitude
Observer zenith angle at target	Observer-target range
True observer-target range	Solar zenith
Ground albedo	Visibility
Relative azimuth angle of observer	Clutter parameter

Most of these variables are self-explanatory. *Altitude* is the minimum altitude reached by the tangential path between target and detector. The *true observer-target range* and *range* options describe the distance between target and detector. The latter should be used for paths which leave the Earth's atmosphere. For the purposes of the atmospheric model used, the atmosphere is essentially 30km thick, but minor corrections are made up to an altitude of 100km. This option should be used in simulations where surface or detector altitude is varied above 100km. The *relative azimuthal angle* is defined for the observer relative to the azimuth of the Sun, with 180° corresponding to an observer standing directly between the Sun and the object. *Clutter* is a measure of the spatial and/or temporal variation in the background radiance, a primitive noise model. Since the resolution of the model is effectively limited to a maximum of two pixels, object and background, only a rough approximation is available. The Clutter Parameter is used in conjunction with the Clutter Emissivity and Clutter Temperature to provide an approximation of the effects of this variable.

A typical simulation involves three phases. Firstly, the simulation must be configured with the required parameters. The suite's user-interface is provided by the SENSIN program. This program presents the simulation variables on a number of menu screens, allowing the definition of the object and detector characteristics. A separate set of menu screens containing the definition of the atmosphere may also be accessed where necessary.

Secondly, the atmospheric model program (SENTRAN) must be run. This section is not required if only the spectral response of the detector is to be calculated. The output from this program is then passed as the input to the Detector Model (SENSAT).

The final results are presented in both textual and graphical forms. Two output files (SENOUT.FLn and SENOUT.PRN) are produced. The .FLn (n is a number) files contain the raw output data for the graph plotting program. The .PRN file contains the same information in a more user-friendly format. The syntax of the .FLn files is such that it is relatively simple to append further data analysis and processing programs to the suite as supplied. The .PRN file is designed for use as the end point of an evaluation. It is the intention to identify areas of interest from the graphical plots, and then to extract the relevant data from the .PRN file. For second and subsequent simulations, the existing SENOUT.PRN file is overwritten, due to size constraints, but up to 7 .FLn files are retained, before being overwritten in chronological order.

The suite is provided with a graph-plotting routine, allowing the reproduction in hardcopy of any of the plots displayed on the screen by the SENSAT program.

6.2.2 Models Incorporated into the Package

6.2.2.1 Modelling of Targets

Targets in SenSAT are represented simply. Unlike the Durham Empirical and Physical Models described in chapter 2, the target is not modelled in the strictest sense, in that its behaviour is not predicted from basic principles. A target is defined in terms of area, temperature and emissivity. The first two are constants, and can be measured for a physical surface. For the purposes of the model, the target emissivity can be defined as a function of the wavelength of the emitted radiation. From these three parameters, the instantaneous thermal behaviour of the surface can be calculated.

A target is defined as any object or background falling within the field of view of the detector. The model allows the geometry of the target configuration to be represented in a number of ways. The simplest option is to have no targets in the Instantaneous Field Of View (IFOV), corresponding to a sensor looking out to space. A single target occupying the whole IFOV is essentially just a background. The final two options are for two or three targets in view respectively. When using these two options, target 1 is regarded as the background, and is assumed to fill the IFOV. Targets 2 and 3 (when incorporated) can be situated at the same altitude as the background, or closer to the detector. The choice is available to look at a target from above or below, with the calculated radiance taking into account reflection off the Earth or direct transmittance from an extra-terrestrial source. Target 2 can also be defined to have a wavelength-dependent emissivity. Target 3, when incorporated, is

set to be an emitter of radiation and not a reflector. If the emitting-target option is implemented, then the emissivity of target 2 is defined by $\varepsilon(\lambda) = $ constant. The program does not allow for the option of having the emitter present without an associated target 2. Should this option be required, then target 2 should be set to provide a negligible contribution by setting it to have a very low temperature (100K), and small area (<0.001% of the IFOV).

The wavelength dependence of the target emissivity is defined as one of six functions, the first of which defines a constant emissivity surface. There are also four pre-defined surface emissivity functions, representing asphalt, meadow, sand and sea surfaces. Unfortunately, there is no direct method of comparing the emissivity functions of these surfaces. General trends can be inferred from the results of changing only the target type between simulations. However, the results are of limited value. The sixth option allows the user to define the surface emissivity function, in an external file.

For sea surfaces, SENSAT incorporates the Cox-Munk model, which describes the reflection of solar radiation as a function of the surface of the sea. In calm conditions, the reflection is predominantly in the direction of specular reflection (ie. no scattering). For rougher surface, signified by increased windspeeds, the reflected radiation is scattered around this direction.

6.2.2.2 Modelling of the Atmosphere

The atmosphere is modelled using SENTRAN. This is a SENSAT-modified version of the standard LOWTRAN-7 code. The model is used to calculate the

transmittance and radiance of the atmosphere, and also to introduce the effects of scattered solar radiation. The model has been modified to include the following:

- A wavelength and observation angle dependent surface albedo

- Diffuse and specular reflection of direct solar radiance

- Reflection off non-horizontal surfaces

- Reflection off surfaces at non-zero height above ground

The properties and composition of the atmosphere vary with geographical location and season. For this reason, SENSAT is supplied with six pre-defined atmospheres as follows:

- Tropical Model (15°N latitude)

- Midlatitude Summer (45°N, July)

- Midlatitude Winter (45°N, January)

- Subarctic Summer (60°N, July)

- Subarctic Winter (60°N, January)

- 1976 U S Standard Model

The principal difference between summer and winter aerosols is the base height of the troposphere. The seasonal aerosol used for any given model may be varied. The seventh option is for a user defined atmosphere. For this option, the composition of a series of layers within the atmosphere must be specified.

In addition to defining the general composition of the atmosphere, variations can be made to the individual altitude profiles of a number of the gases in the atmosphere, namely water vapour, ozone, methane, nitrous oxide and carbon

monoxide. Profiles for these gases are included in the defined atmospheres, but can be altered to the profile for a different atmosphere or the user defined option. This allows for ultimate versatility in defining the atmospheric composition.

Within the boundary layer (altitude < 2km), the atmosphere is also influenced by the ground, and SENTRAN incorporates a number of aerosols, representing rural, urban, fog and desert conditions. The default values for the extinction distances associated with these aerosols can be overridden. In addition, an option exists for a tropospheric aerosol, representing very clear conditions. In this case, the influence of the ground is negligible.

High altitude (tropospheric) aerosol conditions can be significantly influenced by volcanic eruptions. For simulations involving paths through the upper atmosphere (altitude > 30km), the extent to which this influence is modelled can be defined.

6.2.2.3 Modelling of the Sensor

The third program run in a typical simulation is the SENSAT program itself. This is primarily concerned with modelling the effects of the detector components on the output signal. The detector type itself may be chosen from a list of twenty-four preset spectral response functions (relative response as a function of wavelength) or a user defined function. A number of the detectors modelled by the program can be used in conjunction with filters to further modify their spectral responses. The facility exists within the program to plot the relative response of a sensor throughout the wavelength range covered.

As well as spectral response, several of the physical properties of the detector can be defined, including the Peak Detectivity (D*), Peak Responsivity and Optical

Transmittance. A detector element is assumed to be a square, and its size is defined by the length of one edge. In addition, the angular field-of-view can be defined.

6.3 Sensitivity Analysis

A sensitivity analysis was carried out using SenSAT, in order to investigate the capabilities of the software, and to determine which parameters significantly affect the results produced by the model. A number of example cases are reproduced below.

6.3.1 Case 1. Variation of Object Temperature Against a Constant Background

From the list of pre-defined sensors, the *Bendix Scanner* was chosen for this simulation, because its spectral sensitivity curve, $\varepsilon(\lambda)$, as shown in figure 6.1, most closely matches that of the KT19 radiometers as used in the Durham-built systems. The results will, therefore, have some meaning for future practical work. The sensor was used in conjunction with a spectral bandpass filter, giving a resultant spectral range of 7.7-14.0μm and a 2° field-of-view was defined, again for consistency with the KT19 radiometers.
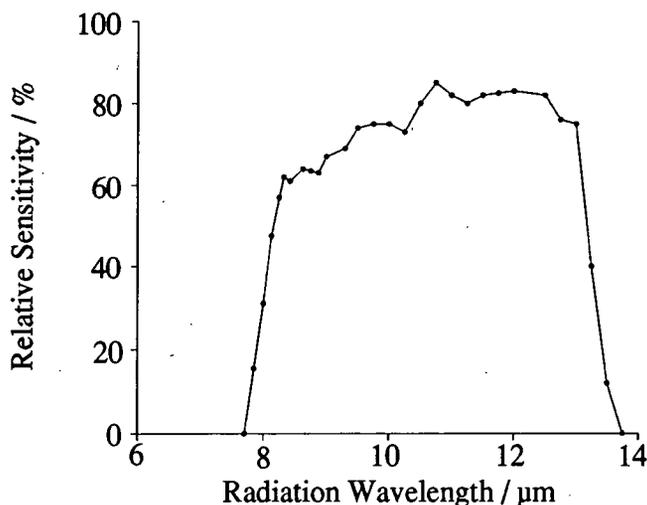
Fig.6.1. Spectral Sensitivity of Bendix Scanner

The target was defined as a 20m² asphalt area in a grass field, which is assumed to be large enough to cover the remainder of the field-of-view. This is similar to targets previously observed with the Durham radiometers. The observer altitude was used as the independent variable, incremented from 100m to 1000m in steps of 100m. The target altitude was set at 0 metres. Observer zenith angle was used as the second independent parameter, with results recorded for angles of 180° (observer vertically above target) and 135° (observer at 45° from the zenith).

The atmospheric composition was set to correspond to a midlatitude summer in a rural aerosol with no cloud cover. Results were calculated for systems under these conditions for asphalt targets at different temperatures against a constant temperature background, and are shown in figures 6.2 and 6.3, and tabulated fully in Appendix C. The background (grass) temperature was set to be 293.2K (20°C), and the target (asphalt) temperature was incremented from 298.2K to 313.2K in steps of 5K. A simulation was also carried out for a grass target with no asphalt present, as a control.
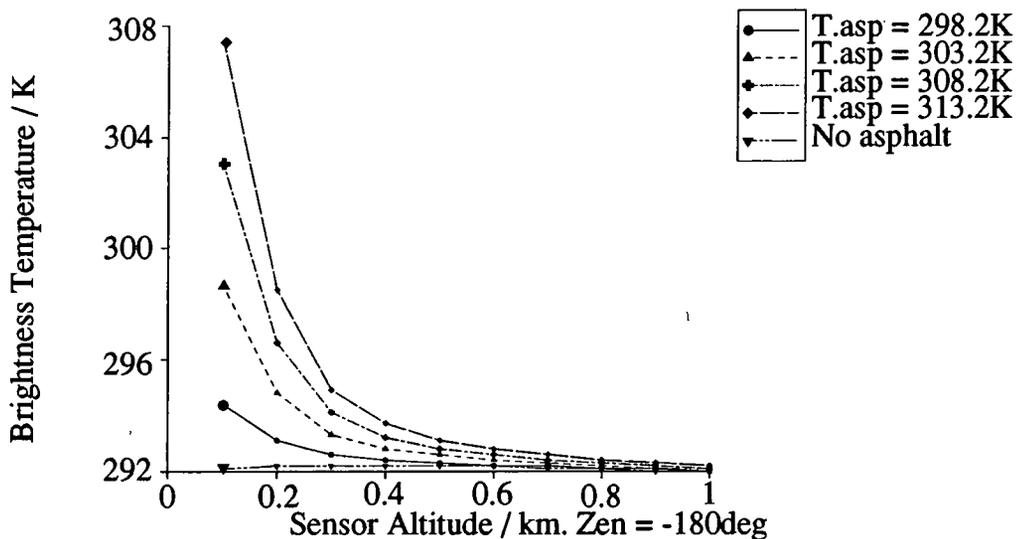
Fig.6.2 Brightness Temperature as function of Sensor Altitude for asphalt targets of different temperatures.
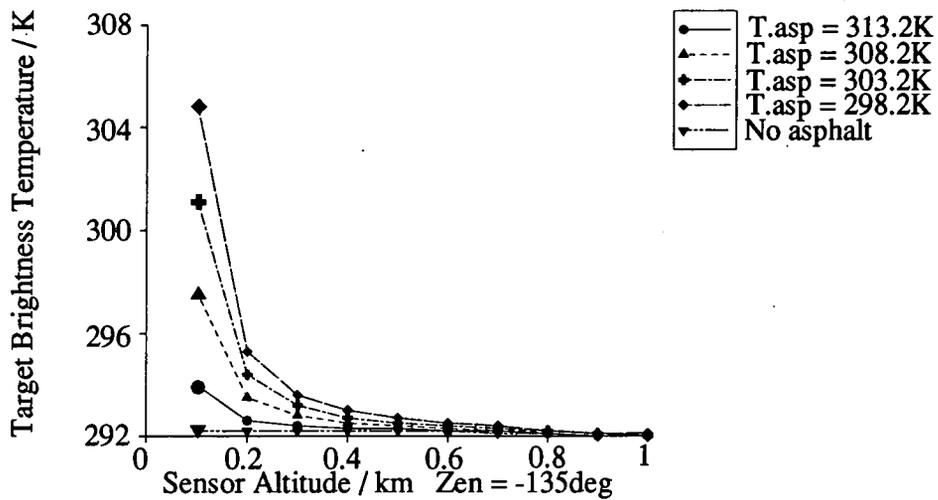
Fig.6.3 Brightness Temperature as function of Sensor Altitude
for asphalt targets of different temperatures

As would be expected, the results converge on this control set at higher altitudes. For altitudes where the brightness temperature difference between the measurements with the target present and absent is greater than the accuracy of the sensor, the target is taken to be detected. For the 298.2K asphalt target, the net temperature difference between the asphalt target being present and absent is plotted in figure 6.4. The fit to the data is provided by a Chebyshev polynomial, which is chosen to provide the smallest maximum error between the data and the polynomial.
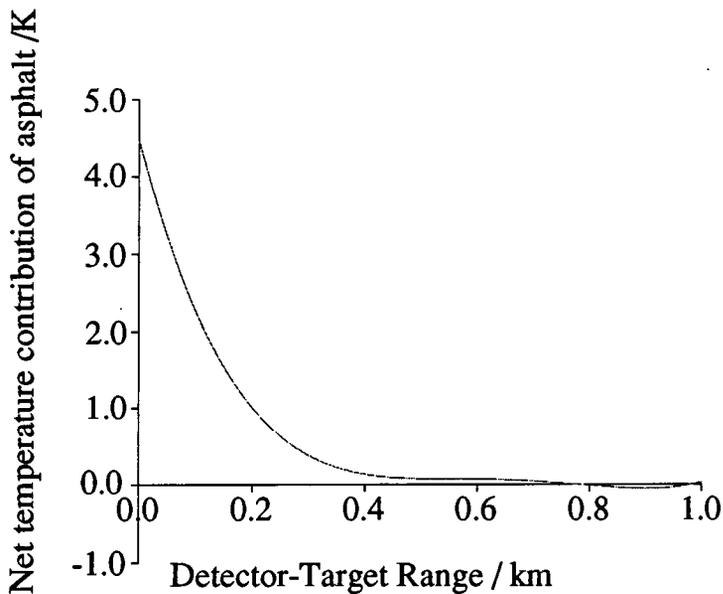
Fig.6.4. Chebyshev fit for net temperature contribution of asphalt at 298.2K
as function of detector-target range

72
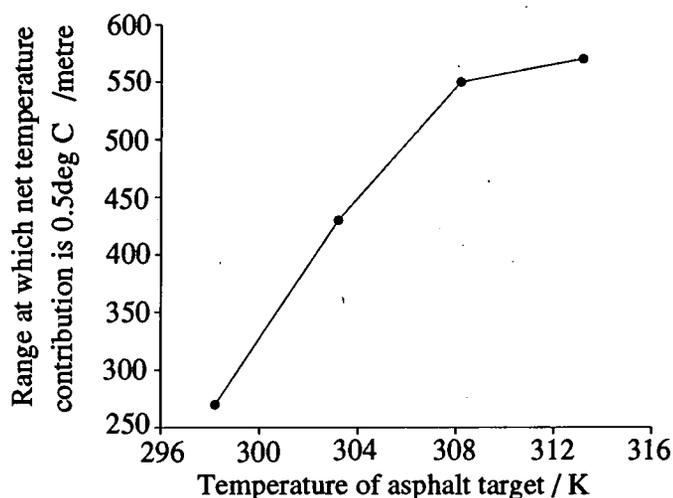
Fig 6.5. Detection Ranges as function of target temperature
for asphalt target on 293K grass background.

No estimates of appropriate sensor accuracy are provided for the SenSAT
detectors, but the figure quoted by the manufacturers for the KT19 radiometer is
0.5°C. If this value is used in conjunction with the SenSAT results, then it would
suggest that an asphalt target at 298.2K on a grass background at 293.2K would be
detected at ranges up to approximately 270m. If the temperature of the asphalt is
increased to 303.2K, then the maximum detection range increases to around 430m.
By repeated application of this procedure, then the maximum range for target
detection as a function of target temperature can be defined. This function is shown
in figure 6.5. The similarity between the two higher temperature predicted ranges
may be due to approximations in the calculations. This method gives the maximum
detection range at some level of confidence. This is dependent on the confidence in
the accuracy of the sensor, which is a noise limited quantity. No indication is given
as to whether the quoted value for the KT19 radiometer is a 'standard error'
(normally σ = 0.5°C) or some multiple thereof. Defining the standard error in the
accuracy of the radiometer would allow for the probability of detection of the target
as a function of the range to be determined.

6.3.2 Case 2. Variation of Aerosol Composition According to Season
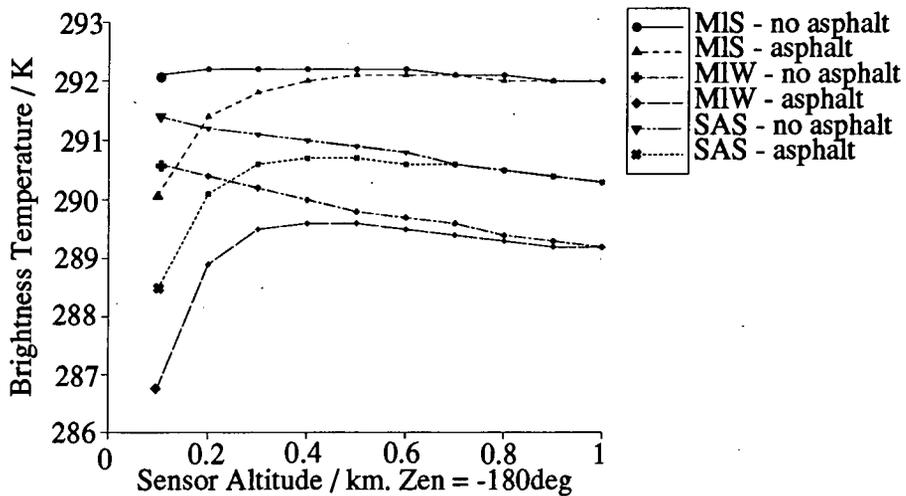
Fig.6.6 Brightness Temperature as function of Sensor
Altitude for Various Aerosols

For this simulation, the same sensor configuration as described in section 6.3.1 was utilised. The geometry of the target and background was also retained, as was the representation of the atmosphere as 'rural'. The temperatures of both the grass and asphalt were maintained at a constant 293.2K. Once again, simulations were carried out with the asphalt target present, and then with it absent, for three different atmospheric compositions, representing summer and winter conditions for a midlatitude aerosol, and a summer arctic atmosphere. The results are shown in figure 6.6. The absolute difference between temperatures recorded under different aerosol conditions demonstrate the effect of the atmospheric composition on transmission of radiation.

By applying the procedures outlined in the previous chapter, the results suggest that the maximum detection range is less for the midlatitude summer atmosphere than the others. This may be interpreted as evidence to suggest that detection ranges are greater under the clearer conditions expected during winter/arctic climates.

6.3.3 Case 3. Variation of Detector Field-of-View at Constant Altitude

For this simulation, the atmospheric parameters and target geometry as described previously were used. Both the target and background were defined to have temperatures of 293.2K. Simulations were carried out for sensors at different range/zenith combinations for a number of sensor field-of-view settings from 0.3° to 3°. The results for a zenith angle of 180° (observer directly above target) and a range of 300 metres are shown in figure 6.7.
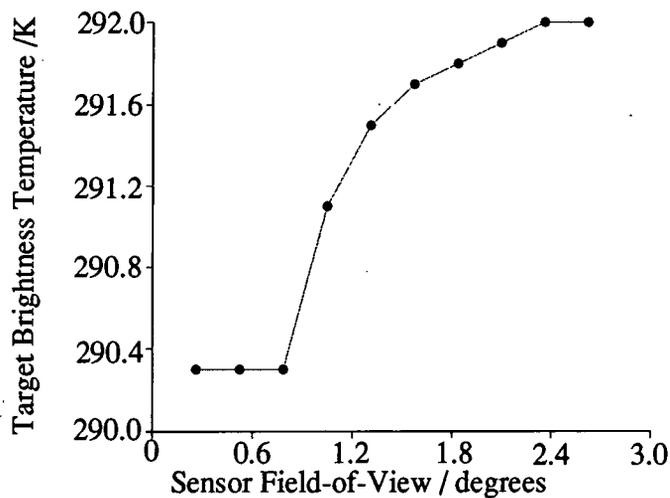
Fig.6.7. Brightness Temperature as function of
Sensor field-of-view. Sensor Altitude = 300m

The results show that for this particular configuration, a sensor with a field-of-view less than approximately 0.85° centred on the target will detect only the signal from the asphalt. As the field of view increases, so does the proportion of the area under observation occupied by the grass background, and the total brightness temperature increases accordingly. This tends to a limit as the asphalt target becomes a point source of negligible area. This demonstrates that the ideal sensor field-of-view for this geometry ~0.85°. A comparison of simulation runs for asphalt and grass targets occupying the full detector field of view shows higher brightness temperatures for the grass target, which corroborates the above result.

6.4 Incorporation of SenSAT with further software packages

6.4.1 Target Model

The particular strengths and weaknesses of the ONTAR/SenSAT suite have been demonstrated during the evaluation of the software.

The detector and atmosphere models are flexible, and can be tailored to meet most requirements. The major limitation of the SenSAT package is the absence of a true target model. The direct measurement of target temperature by contact means may not always be possible. Under such circumstances, it is desirable to be able to estimate the temperature of a surface from parameters which may be remotely measured, such as meteorological conditions and physical constants, defining the properties of the target material. This requirement may be achieved by incorporating a target temperature prediction model, such as the DGPM (Hughes *et al*, 1993). These temperatures may then be combined with the SenSAT atmospheric and detector sub-models.

The incorporation of results from the DGPM into the SenSAT suite can be achieved by one of two methods. It is trivial to run the two models separately, and to transfer results from one to the other, using the existing SENSIN interface. This would allow preliminary investigations of the compatability of the two models. This is unsatisfactory for a number of reasons. SenSAT is a DOS package, and the DGPM is currently implemented under UNIX.

An attractive solution involves merging the two models on a single platform. This can be achieved by installing PC hardware or emulating software in an Acorn computer, and establishing SenSAT. The availability of an ethernet network already

```
┌─────────────────────────────┐
│ Parameter Input Interface   │
│ for SenSAT and Durham       │
│ General Purpose Model       │
│                  RISC OS│   │
└─────────────────────────────┘
        │                │
        ▼                │
┌──────────────────┐     │
│ Durham General   │     ▼
│ Purpose Model    │
│                  │
│      UNIX (HP-UX)│
└──────────────────┘
        │
        ▼
┌─────────────────────────────┐
│ Data Arrangement Interface  │
│ for SENSAT suite            │
│                             │
│                  RISC OS│   │
└─────────────────────────────┘
        │
        ▼
┌─────────────────────────────┐
│ PC SenSAT - SENTRAN         │
│ and SENSAT models           │
│                             │
│                      DOS│   │
└─────────────────────────────┘
        │                │
        ▼                │
┌──────────────────┐     │
│ Probability of Detection   │
│ Model            │     ▼
│                  │
│      RISC OS│    │
└──────────────────┘
        │
        ▼
┌─────────────────────────────┐
│ Durham University           │
│ Thermal Simulator           │
│                             │
│                  RISC OS│   │
└─────────────────────────────┘
```
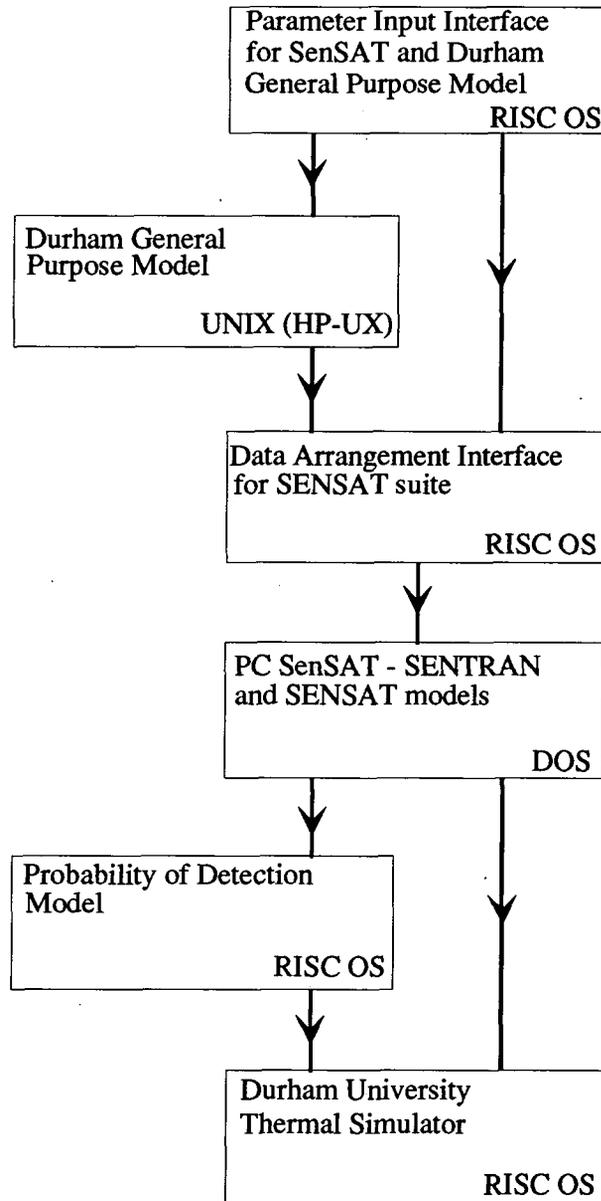
Fig.6.8.Proposed Structure for a combined modelling
and display software suite

allows for the DGPM to be run remotely from an Acorn machine. Thus it appears

possible to operate all of the software from a single computer, with the management

and file-handling processes being carried out by the native RISC OS (Reduced

Instruction Set Computing Operating System), and the modelling requirements being

dispatched, if necessary, to a third party system. The facility already exists for

RISC OS machines to produce output in a DOS readable format to a separate DOS

partition on the hard disk. The requirement is therefore to produce a file of the format

accepted by the SENTRAN sub-model, which contains the output from the DGPM. This involves replacing the SENSIN user interface. The new interface will have to produce all of the data required of the original, in addition to the inputs for the DGPM. The output from the DGPM must then be merged with the remainder of the input data to form an input file of the format required by the SENTRAN sub-model. This format is detailed in the SenSAT Technical Manual. The SENTRAN and SENSAT sub-models would then be run under DOS as before. The structure of the proposed combined suite is outlined in figure 6.8. It is proposed to provide such a platform on an Acorn A5000 computer with a hardware card installed to provide the machine with an 80486 PC processor for the SENSAT operations, and ethernet connectivity to a UNIX environment for the DGPM.

6.4.2 Modelling Probability of Detection

The outputs from a SenSAT simulation are expressed in terms of some variable which is related to the response of the sensor. Comparison of the outputs for simulation scenes with some target present and missing form the basis for developing a probability of detection of the target under a particular set of conditions. This probability has particular use in search applications, where an object may or may not be present, or its location is unknown. A model is therefore required for the calculation of a detection probability, based on signal strengths, as output from SenSAT, and physically measurable properties of the object's environment (range, size etc.). A method based on the accuracy of the sensor has been outlined in section 6.3.1. The basis for an alternative method, based on a Minimum Resolvable Temperature Difference (MRTD) model may lie in a combination of two simple concepts. An object may be discerned from its background when the contrast between the two is significant enough for the detector to show some change when moving from background to target observation. It is therefore necessary to define the

probability of detection as a function of the contrast, and by extension, as a function of the strength of the signal from target and background. Since Johnson's work in the 1950s (Johnson, 1958), the number of discernible contrasting elements across some target/background have been used to determine the level of detection/recognition in the scene. Using such a method requires a knowledge of the minimum contrast detectable by the sensor. This will be based on the temperature, or generically, the luminance, of the target within the field-of-view of the detector. A minimum resolvable luminance difference (MRLD) model is described by Karim, Gao and Zheng (1991) which may satisfy this requirement. This method allows for the possibility of assigning probabilities to the different levels of detection (detection, recognition, orientation and identification)

6.4.3 Display Software

Previous work in Durham has included the development of a graphical display package (McComb, Smith, Turver, 1991), the Durham University Thermal Simulator (DUTS). DUTS provides a false colour image of a scene based on the temperatures of targets in view, and allows the scene to be viewed from various viewpoints. Currently, work on DUTS has been limited to representation of meteorological data and Durham Empirical Model results. In the future, DUTS, or another graphical display package, may provide the basis for a detailed display interface, based on the probability of detection of various targets against some background.

6.5 Summary

SenSAT is a combined detection model package, which simulates the effects of the atmosphere and a detector on infrared radiation emitted by a target. Both of these elements are modelled in some detail, and can be configured to individual requirements. It is thus a useful tool in optimizing the performance of a particular sensor for a given set of circumstances.

It does not, however, include a true model for predicting target temperatures from physical parameters. The Durham General Purpose Model satisfies these requirements, and may be incorporated into the suite by means of a new input interface program.

The results from SenSAT are based on the effects on detector output of changes of an independent variable. The format of these results is such that it is possible to further process and manipulate the data. One such possibility is the development of a probability of detection as functions of range, target and background temperatures etc.. The calculation of such probabilities is dependent on knowledge of the accuracy of the detector in use.

The further incorporation of the combined SenSAT/DGPM with a graphical display package would allow a pictorial representation of a scene to indicate objects by probability of detection from a given viewpoint.

Chapter 7. Conclusions and Future Work

7.1 Introduction

This thesis describes work on a broad range of topics. This work has fallen into three distinct areas; the refurbishment of the radiometers, the empirical modelling, and investigations into detection models.

The radiometer refurbishment was carried out in order to provide a measurement capability in the 2-5µm waveband in the infrared spectrum, and to enhance the existing video and 8-14µm waveband capabilities.

The validity of the empirical model for dealing with layered surfaces was demonstrated by analysis of the dataset from the Ouston-II experiment - a more challenging trial than previous applications of the model.

The composition of a generic detection model is described, and potential methods of developing a model suitable for use with the systems built in Durham have been examined. A commercial detection model package (SenSAT) has been investigated, with a view to incorporating it with the Durham General Purpose Model.

In this chapter, the prospects for future work in these three and related fields are assessed.

7.2 Future Improvements to Measuring Equipment

A number of features were incorporated into the refurbishment of the prototype radiometer which were not subsequently implemented in the rebuilt units. As detailed in chapter 2, the Durham Empirical Model uses an estimate of the sky radiometric temperature, and calculates this as the average of a number of temperature readings of sky targets. The control and logging software for the prototype radiometer was modified to give the option of making such a scan automatically at the end of the user defined target scan. The controlling A310 computer in the prototype unit was also modified to include a video digitization card. This allowed the video signal from the camera to be passed to the computer, and snapshot images stored as Sprite files. This tool provides the facility to store a visual record of a scan on disk with the radiometric data. More importantly, it also provided a potentially accurate method of estimating percentage cloud cover, if used in conjunction with the sky scan routine described above.

7.3 Further Work on Target Models

Work is currently underway to produce a physical model to describe the temperature profile through a layered textile suspended above the ground surface. The data acquired from the trial at Ouston 1992, as described in this thesis, will serve towards the validation of this model. It may prove desirable to carry out further experiments should it be identified that specific data is required and not currently available.

The Durham Empirical Model has been successfully validated for use in describing the thermal behaviour of textile layers suspended over simple surfaces.

7.4 A Detailed Detection Model

The work done on detection modelling has highlighted the desirability of producing a model particular to the system in use with Durham radiometers and the type of observations typically undertaken. As described in chapter 5, a complete detection model incorporates three sections; modelling of the surface, atmosphere and detector. A number of models, describing a wide variety of surfaces, have been developed in Durham, and would form the basis for the development of an 'end-to-end' detection model. A detector model based on the KT19 radiation thermometer could be developed, to relate the output of the unit to the observed temperatures. At the most basic level, the simple calibration equation for the unit, as described in chapter 3 will serve this purpose. Any detector model will, at least initially, probably be an empirical model, based on observations of the behaviour of the unit under various conditions, as opposed to a physically sound model based on detector characteristics such as the detectivity and noise. The role of an atmospheric model in the development of a detection model is currently unclear. The Durham-built radiometers are typically used in observations of objects within about 100 metres of the unit, with the exception of sky targets which are a special case. At such short ranges, the attenuating effects of the atmosphere are relatively insignificant, and can be approximated by an exponential decay function if so desired. If a full-scale atmospheric model was required, with a view to using the system for longer-range measurements, then a commercial model, probably LOWTRAN, could be incorporated without much difficulty.

The next step would be to develop a model to express a probability of detection for a given object against some background as a function of the output from a detection model. A suitable detection model would be SenSAT, as described in chapter 6. A number of suitable methods for determining Probability of Detection have also been described in chapter 6.

Appendix A.

Radiometer Calibration Details

These data correspond to figures 3.4 to 3.10 on pages 22-9. They provide the raw data for the determination of the fields-of-view and calibration equations for the KT19 and CE825 radiation thermometers, and for the determination of the 'warm-up' time of the CE825 thermometer.

1.Field of View of KT19 Radiation Thermometer.

Table A.1.a. Azimuthal Field of View

Off-axis angle degrees	Radiometer Output °C
-7.325	15.9
-6.604	16.0
-5.883	16.1
-5.164	16.3
-4.445	16.2
-3.727	16.2
-3.009	16.3
-2.292	16.4
-1.576	17.3
-1.433	18.6
-1.289	20.8
-1.146	24.3
-1.003	27.0
-0.859	31.7
-0.716	36.5
-0.573	40.1
-0.430	44.4
-0.286	47.3
-0.144	48.8
0.000	49.2
0.144	47.6
0.286	44.4
0.430	39.9
0.573	36.2
0.716	31.5
0.859	28.2
1.003	24.7
1.146	20.5
1.289	18.6
2.006	16.6
2.723	16.3
3.440	16.2
4.158	16.2
4.876	16.2
5.595	16.1
6.315	16.1
7.036	16.1

Table A.1.b. Zenithal Field of View

Off-axis angle degrees	Radiometer Output °C
-8.627	15.0
-7.903	15.1
-7.181	15.2
-6.459	15.2
-5.739	15.3
-5.020	15.4
-4.301	15.4
-3.583	15.4
-2.866	15.4
-2.149	15.7
-1.433	19.7
-1.289	23.3
-1.146	28.2
-1.003	35.5
-0.859	43.1
-0.716	52.1
-0.573	59.7
-0.430	66.2
-0.286	72.5
-0.143	76.7
0.000	78.1
0.143	76.5
0.286	72.9
0.430	67.0
0.573	59.7
0.716	51.1
0.859	44.3
1.003	35.3
1.146	29.0
1.289	22.7
1.433	18.0
2.149	15.9
2.866	15.7
3.583	15.5
4.301	15.4
5.020	15.4
5.739	15.4

2. Field of View of CE825 Radiation Thermometer

Table A.2.a. Azimuthal Field-of-View

Off-axis angle degrees	Radiometer Output millivolts
-5.281	265
-4.628	268
-3.975	268
-3.322	274
-2.670	275
-2.019	279
-1.628	335
-1.367	425
-1.107	549
-0.716	698
-0.456	759
-0.326	775
-0.195	789
-0.065	794
0.065	794
0.195	788
0.326	777
0.456	758
0.586	735
0.846	651
1.237	484
1.498	381
1.888	294
2.540	275
3.192	275
3.844	272
4.497	266
5.151	263

Table A.2.b. Zenithal Field-of-View

Off-axis angle degrees	Radiometer Output millivolts
-9.861	254
-9.134	235
-8.410	229
-7.686	229
-6.964	228
-6.243	228
-5.523	227
-4.804	229
-4.086	242
-3.368	256
-2.651	256
-2.364	256
-2.077	268
-1.934	294
-1.791	329
-1.647	375
-1.504	432
-1.361	492
-1.218	546
-1.074	609
-0.931	668
-0.788	716
-0.645	750
-0.501	784
-0.358	810
-0.215	824
-0.072	836
0.072	839
0.215	830
0.358	811
0.501	798
0.645	745
0.788	704
0.931	636
1.218	506
1.647	323
1.934	264
2.364	242
3.081	242
3.799	240
4.517	240

Table A.3. Calibration curve for low temperature range KT19.
Ambient temperature = 20.8°C

Blackbody Temperature °C	Radiometer Output Voltage Millivolts
24	563
26	573
28	585
30	596
32	608
34	620
36	632
38	643
40	656
45	684
50	718
55	745
60	775
65	806
70	835
75	867
80	894
85	927
90	954
95	989
100	1012

Table A.4. Calibration curve for standard temperature KT19.
Ambient temperature = 22.9°C

Blackbody Temperature °C	Radiometer Output Voltage Millivolts
28	519
30	529
32	541
34	554
36	567
38	580
40	593
45	625
50	660
55	689
60	721
65	754
70	788
75	822
80	851
85	887
90	916
95	954
100	979

Table A.5. Indepencence of radiometer output temperature from ambient temperature.

| Ambient Temperature | Radiometer Output voltage for | |
| | $T_{bb} = 45°C$ | $T_{bb} = 70°C$ |
	millivolts	
13.1	688	837
14.4	688	836
16.9	687	835
20.7	684	835
24.2	685	835
25.3	684	835

Table A.6. Calibration curve for CE825. Ambient temperature = 24.0°C

Blackbody Temperature °C	Radiometer Output Voltage Millivolts
30	574
32	613
34	650
36	689
38	725
40	765
42	801
44	839
45	862
46	881
48	920
50	969
52	999

Table A.7. CE825 output voltage as function of time from power-up.

Time since Power up Seconds	Output Voltage Millivolts
0	999(max)
130	999
160	990
175	982
190	973
205	964
220	952
235	944
250	937
265	927
280	917
295	908
310	898
325	895
340	886
355	880
370	872

Time since Power up	Output Voltage
Seconds	Millivolts
385	866
400	858
415	852
430	844
445	838
460	831
475	825
490	819
505	813
520	807
535	800
550	794
565	789
580	784
595	778
610	772
625	767
640	761
655	757
670	751
685	747
700	741
715	737
730	732
745	727
760	723
775	718
790	715
805	710
820	706
835	701
850	698
865	692
880	689
895	684
910	679
925	676
940	672
955	669
970	664

Time since Power up	Output Voltage
Seconds	Millivolts
985	661
1000	660
1015	656
1030	653
1045	651
1060	648
1075	646
1090	643
1105	641
1120	638
1135	635
1150	631
1165	629
1180	626
1195	624
1210	621
1225	618
1240	616
1255	615
1270	612
1285	610
1300	607
1315	607
1330	605
1345	603
1360	600
1375	598
1390	597
1405	596
1420	596
1435	595
1450	595
1465	595
1480	595

Appendix B.

Validation of Empirical Model for Textile Layer Surfaces

Descriptions of the objects studied are stored in target files in the radiometers. In addition to the description of the object surface, the surface azimuth and inclination are also stored for use by the model. These are reproduced below.

Rad.	Target	Description	Azimuth	Inclination
Rad3	5	Grass	000°	000°
	8	Material C inclined	-132°	045°
	9	Material C flat	000°	000°
	10	Tarmac	000°	000°
	11	Material B flat	000°	000°
	12	Material B inclined	-132°	045°
	13	Material A flat	000°	000°
	14	Material A inclined	-132°	045°
	15	Tarmac	000°	000°
	18	Material A flat + grass	000°	000°
Rad4	9	Tarmac	000°	000°
	11	Material D inclined	-132°	045°
	12	Material D flat	000°	000°
	13	Tarmac	000°	000°
	14	Material C flat	000°	000°
	15	Material C inclined	-132°	045°
	16	Material B flat	000°	000°
	17	Material B inclined	-132°	045°
	20	Grass	000°	000°

Table B.1.a Objects observed by Radiometers 003 and 004

Rad.	Target	Description	Azimuth	Inclination
Rad5	7	Grass	000°	000°
	11	Material D flat	000°	000°
	12	Material D inclined	-132°	045°
	13	Material C flat	000°	000°
	14	Material C inclined	-132°	045°
	15	Tarmac	000°	000°
	16	Material B flat	000°	000°
	17	Material B inclined	-132°	045°
	18	Material A flat	000°	000°
	19	Material A inc. + grass	048°	045°
	20	Material A flat + grass	000°	000°
	23	Grass	000°	000°

Table B.1.b Objects observed by Radiometer 5

Target	Layer Albedo	Layer Coverage	Material
A/AII	0.294	67.5%	Polyurethane coated nylon
B	0.440	75%	Acrylic coated nylon
C	0.314	63%	Polyurethane coated nylon
D	Not known	Not known	Not known

Table B.2 Textile Target Descriptions

Day No.	Remarks
235	Solar Radiation Peak at 600W/m², but much intermittent cloud cover, resulting in troughs as low as 100W/m². Air temperature varied from ~10°C to ~16°C. Windspeed peaked at 5m/s. Very small amount of rain in afternoon.
236	Slightly more Solar Radiation, up to 650W/m², but similar cloud cover effects. Corresponding increase in temperature, with variation from 12°C to 20°C. The wind was relatively constant between 3m/s and 5m/s. No rain.
237	More cloud than previous days, resulting in only 2 sharp spikes of solar radiation, but one of these reached 800W/m². Very small air temperature variation from 15°C to 19°C. Almost no wind. No rainfall.
238	High Solar Radiation readings up to 700W/m², with few troughs, indicating little cloud cover. Air temperature ranged from 12°C to over 20°C. Little wind. No rain.
239	Virtually complete cloud cover all day. Maximum solar radiation below 200W/m². Air temperature was virtually constant around 14°C. Very little wind. Rain in afternoon.

Table B.3.a Summary of Weather Conditions for Mixed Weather Period

Day No.	Remarks
241	Solar radiation produced a bell-shaped curve, with only a few spikes due to cloud. Solar radiation peaks at 650W/m². Air temperature increases from 10°C at 0800 to a maximum of over 20°C at 1500. There was minimal wind, and no rainfall.
242	Solar radiation produced a perfect bell-shaped curve to a maximum of 600W/m². The air temperature showed similar variation to previous day, remaining constant at night, around 14°C, with a day time maximum of 23°C. Once again, there was little wind and no rain.
243	Again, the solar radiation curve was near-ideal, with the result of a similar air temperature curve, but with a smaller variation from 12°C to 20°C. Again, there was little wind and no rain.
244	Smooth solar radiation curve, but smaller magnitude than previous days. Air temperature varied from 10°C to 20°C. Again, there was no rain and minimal wind.
245	Appears to have been cloud cover in the morning. The maximum solar radiation was 550W/m². Air temperature varied little from 13°C to 17°C. Yet again, there was no rain and little wind.
246	Solar radiation peaked at 600W/m², but again appears to have been attenuated by morning cloud.
247	Solar radiation curve is ragged, and relatively low in magnitude, having a peak at 500W/m². Little variation in air temperature, from 12°C to 20°C. Again, no rain and little wind.

Table B.3.b.i Summary of Weather Conditions for Excellent Weather Period

Day No.	Remarks
248	Minimal solar radiation, with peak at 300W/m². Very small air temperature variation, up to a maximum of 19°C. Wind was slightly stronger than previous days, but again, no rain.
249	Solar radiation curve was almost ideal, except for a spike around 1300, and had a maximum of 600W/m². Air temperature varied from 7°C to 15°C. Wind was negligible once again, and there was no rain.
250	Solar radiation showed very smooth curve upto 600W/m², and air temperature varied smoothly between 6°C and 20°C. The wind was stronger than previous days, but again there was no rain.

Table B.3.b.ii Summary of Weather Conditions for Excellent Weather Period

Radiometer	Target	Excellent Weather		Mixed Weather	
		Coeff.	Error	Coeff.	Error
3	5	0.01607	0.00073	0.01562	0.00068
	8	0.00729	0.00055	0.00392	0.00052
	9	0.00522	0.00052	0.00642	0.00038
	10	0.01162	0.00104	0.01574	0.00067
	11	0.00371	0.00050	0.00609	0.00040
	12	0.00684	0.00056	0.00292	0.00046
	13	0.00827	0.00056	0.00872	0.00042
	14	0.01247	0.00069	0.00760	0.00068
	15	0.01356	0.00106	0.01843	0.00077
	18	0.01461	0.00067	0.01025	0.00055
4	9	0.01335	0.00047	0.01340	0.00053
	11	0.00787	0.00065	0.00500	0.00062
	12	0.00663	0.00048	0.00728	0.00034
	13	0.01384	0.00047	0.01658	0.00057
	14	0.00857	0.00040	0.00869	0.00036
	15	0.00717	0.00058	0.00590	0.00053
	16	0.00200	0.00042	0.00246	0.00028
	17	0.00752	0.00063	0.00403	0.00039
	20	0.01915	0.00053	0.01750	0.00065
5	7	0.01258	0.00031	0.01188	0.00041
	11	0.00863	0.00026	0.00829	0.00032
	12	0.00343	0.00044	0.00403	0.00052
	13	0.00926	0.00030	0.00919	0.00035
	14	0.00136	0.00048	0.00247	0.00054
	15	0.01717	0.00042	0.01790	0.00063
	16	0.00337	0.00023	0.00340	0.00024
	17	0.00379	0.00045	0.00207	0.00047
	18	0.00985	0.00031	0.01074	0.00034
	23	0.00985	0.00044	0.01095	0.00043

Table B.4   Solar Radiation Coefficients for best fits of model to various
surfaces during both weather periods.

| | | Excellent Weather | | Mixed Weather | |
Radiometer	Target	Coeff.	Error	Coeff.	Error
3	5	-1.71934	0.30695	-1.27239	0.25405
	8	-0.67625	0.19352	0.10006	0.13748
	9	-0.45980	0.21811	-0.82292	0.14262
	10	-1.48084	0.43765	-1.48891	0.25173
	11	-1.17782	0.21031	-1.07221	0.15000
	12	-1.71393	0.19744	0.00401	0.12105
	13	0.00479	0.23434	-0.62478	0.15720
	14	-0.56213	0.23848	0.79126	0.17955
	15	-0.87437	0.44780	-1.22753	0.04108
	18	-1.04039	0.28075	-0.64414	0.20429
4	9	-4.10143	0.18170	-1.41592	0.19674
	11	-1.27396	0.17777	0.68725	0.16130
	12	-1.67782	0.18655	-0.48937	0.12610
	13	-3.55683	0.18353	-1.06742	0.21025
	14	-3.13441	0.15696	-1.16520	0.13451
	15	-1.12285	0.15869	0.45255	0.13701
	16	-2.50331	0.16306	-0.98873	0.10327
	17	-3.06016	0.17195	-0.78967	0.10283
	20	-3.32288	0.20724	-1.50860	0.23856
5	7	-2.55970	0.11001	-1.22589	0.14856
	11	-1.85105	0.09265	-0.76028	0.11601
	12	-0.60495	0.10124	0.51700	0.13610
	13	-2.03954	0.10870	-0.75010	0.12810
	14	-1.02604	0.11161	0.58192	0.13911
	15	-2.37050	0.14971	-1.14745	0.23233
	16	-2.13815	0.08032	-0.98416	0.08873
	17	-1.83993	0.10395	-0.12203	0.12086
	18	-2.26942	0.10886	-0.54270	0.12621
	23	-2.25943	0.15821	-0.93296	0.15807

Table B.5 Air Temperature Coefficients for best fits of model to various surfaces during both weather periods.

Radiometer	Target	Excellent Weather		Mixed Weather	
		Coeff.	Error	Coeff.	Error
3	5	-0.56817	0.12580	-0.20016	0.06657
	8	0.20546	0.07209	0.08425	0.04089
	9	-0.49604	0.08967	-0.06437	0.03737
	10	-0.12811	0.17931	-0.07877	0.06596
	11	-0.24671	0.08619	-0.07883	0.03931
	12	0.30167	0.07355	0.03381	0.03600
	13	-0.83190	0.09604	-0.10511	0.04119
	14	0.52516	0.08884	0.05647	0.05340
	15	0.00821	0.18352	0.03801	0.07534
	18	-0.92382	0.11506	-0.14827	0.05353
4	9	0.22583	0.09140	-0.11237	0.05536
	11	0.90428	0.07725	0.07540	0.04840
	12	-0.37441	0.09384	-0.06044	0.03548
	13	0.25078	0.09232	-0.13207	0.05916
	14	-0.58832	0.07895	-0.20406	0.03785
	15	0.34426	0.06896	-0.12277	0.04111
	16	-0.72457	0.08202	0.02163	0.02906
	17	-0.67646	0.07472	0.12147	0.03086
	20	-1.05160	0.10425	-0.00645	0.06712
5	7	-0.16930	0.06547	-0.05520	0.04261
	11	-0.41716	0.05514	-0.19762	0.03328
	12	0.36824	0.05348	-0.00002	0.04089
	13	-0.17273	0.06469	-0.22968	0.03674
	14	0.30011	0.05897	-0.10146	0.04180
	15	-0.27144	0.08910	-0.29035	0.06664
	16	-0.24590	0.04780	-0.03405	0.02545
	17	0.45368	0.05492	0.14707	0.03631
	18	-0.36010	0.06479	-0.39343	0.03620
	23	-0.39248	0.09416	-0.09258	0.04534

Table B.6 Wind speed Coefficients for best fits of model to various surfaces during both weather periods.

| | | Excellent Weather | | Mixed Weather | |
Radiometer	Target	Coeff.	Error	Coeff.	Error
3	5	-0.72000	0.15494	-1.08971	0.15701
	8	-0.80575	0.09099	-0.88837	0.09693
	9	-0.00850	0.11045	-0.52290	0.08815
	10	0.98170	0.22092	0.22742	0.15558
	11	0.04854	0.10616	-0.59108	0.09271
	12	-0.76828	0.09283	-0.73406	0.08535
	13	0.16207	0.11829	-0.38250	0.09716
	14	-0.89351	0.11212	-0.77393	0.12660
	15	0.37018	0.22604	0.04108	0.17770
	18	-0.18514	0.14171	-0.44256	0.12626
4	9	3.07662	0.11587	1.04421	0.13740
	11	1.43566	0.11094	0.77243	0.12167
	12	1.77881	0.11896	0.71458	0.08807
	13	3.48414	0.11704	1.46734	0.14683
	14	3.33939	0.10009	1.20139	0.09394
	15	2.52760	0.09904	1.54665	0.10335
	16	1.93774	0.10398	0.36400	0.07212
	17	1.60705	0.10731	0.15245	0.07757
	20	1.95013	0.13215	0.18620	0.16660
5	7	-0.44056	0.09021	-1.13499	0.10767
	11	0.56799	0.07597	-0.50437	0.08408
	12	-0.30237	0.08392	-0.82454	0.10503
	13	0.95425	0.08913	-0.20064	0.09284
	14	1.47738	0.09253	-0.26117	0.10735
	15	2.26049	0.12276	0.21701	0.16839
	16	0.58390	0.06586	-0.76455	0.06431
	17	-0.36559	0.08618	-1.04393	0.09327
	18	1.56782	0.08926	0.64916	0.09148
	23	-0.30194	0.12973	-0.98053	0.11456

Table B.7 Temperature Depression Coefficients for best fits of model
to various surfaces during both weather periods.

103

Radiometer	Target	Excellent Weather Residuals		Mixed Weather Residuals	
		Average	RMS	Average	RMS
3	5	**1.33404**	1.66114	**1.20961**	1.76260
	8	**0.80952**	1.00115	**0.84725**	0.78697
	9	**0.96620**	1.18415	**0.78697**	0.98952
	10	**2.04273**	2.36846	**1.30395**	1.74650
	11	**0.91540**	1.13814	**0.82133**	1.04072
	12	**0.84942**	1.02147	**0.76129**	0.97300
	13	**0.99903**	1.26818	**0.78683**	1.09066
	14	**0.99864**	1.23377	**1.04105**	1.44318
	15	**1.97047**	2.42337	**1.40632**	1.99484
	18	**1.18835**	1.51935	**0.93810**	1.41734
4	9	**1.09338**	1.43776	**1.08936**	1.48233
	11	**1.12056**	1.46331	**0.97952**	1.34239
	12	**0.95610**	1.47614	**0.67239**	0.95011
	13	**1.12034**	1.45223	**1.14817**	1.58412
	14	**0.94590**	1.24915	**0.74997**	1.01346
	15	**0.97311**	1.30628	**0.79146**	1.14023
	16	**0.92022**	1.29023	**0.58875**	0.77808
	17	**0.97154**	1.41540	**0.65097**	0.85578
	20	**1.16712**	1.63981	**1.16133**	1.79737
5	7	**0.80265**	1.19602	**0.75926**	1.14407
	11	**0.74335**	1.00729	**0.62771**	0.89343
	12	**0.88717**	1.17344	**0.78683**	1.14245
	13	**0.88402**	1.18172	**0.71597**	0.98650
	14	**1.00361**	1.29382	**0.84191**	1.16768
	15	**1.23055**	1.62766	**1.29691**	1.78926
	16	**0.64719**	0.87318	**0.52124**	0.68334
	17	**0.94220**	1.20498	**0.75164**	1.01453
	18	**0.91359**	0.93640	**0.71960**	0.97200
	23	**1.16630**	1.72005	**0.77870**	1.21731

Table B.8 Goodness of fit measurements for model representations of measured radiometric data

Appendix C.

PC-SenSAT Sensitivity Analysis

As part of the analysis of the PC-SenSAT software suite, a sensitivity analysis was carried out to investigate the responses of the model to changes in a number of parameters describing all aspects of the sensor-atmosphere-target system. Graphical representations of these data, and interpretations are found in chapter 6. This appendix contains the numerical data produced as output files by SenSAT under a wide range of simulated conditions.

Radiation Wavelength µm	Relative Sensitivity (%)
7.70	0.0
7.85	15.5
8.00	31.0
8.13	47.5
8.25	57.0
8.32	62.0
8.42	61.0
8.63	64.0
8.75	63.5
8.88	63.0
9.00	67.0
9.30	69.0
9.50	74.0
9.75	75.0
10.00	75.0
10.25	73.0
10.50	80.0
10.75	85.0
11.00	82.0
11.25	80.0
11.50	82.0
11.75	82.5
12.00	83.0
12.50	82.0
12.75	76.0
13.00	75.0
13.25	40.0
13.50	12.0
13.75	0.0

Table C.1 Relative Sensitivity of Bendix Scanner (SenSAT detector no.9) as function of radiation wavelength.

Sensor Altitude (km)	Brightness Temperature (K)					Surface Temperature (K)
	298.2	303.2	308.2	313.2	No Asphalt	
0.1	294.4	298.7	303.1	307.5	292.1	
0.2	293.1	294.8	296.6	298.5	292.2	
0.3	292.6	293.3	294.1	294.9	292.2	
0.4	292.4	292.8	293.2	293.7	292.2	
0.5	292.3	292.6	292.8	293.1	292.2	
0.6	292.2	292.4	292.6	292.8	292.2	
0.7	292.2	292.3	292.4	292.6	292.1	
0.8	292.1	292.2	292.3	292.4	292.1	
0.9	292.1	292.1	292.2	292.3	292.0	
1.0	292.0	292.1	292.1	292.2	292.0	

Table C.2 Recorded Brightness temperature for Bendix scanner at various altitudes when viewing asphalt surfaces at different temperatures against a grass background at a constant 293.2K. Sensor Zenith Angle = -180°

Sensor Altitude (km)	Brightness Temperature (K)					Surface Temperature (K)
	298.2	303.2	308.2	313.2	No Asphalt	
0.1	294.0	297.6	301.2	304.9	292.2	
0.2	292.6	293.5	294.4	295.3	292.2	
0.3	292.4	292.8	293.2	293.6	292.2	
0.4	292.3	292.5	292.7	293.0	292.2	
0.5	292.3	292.4	292.5	292.7	292.2	
0.6	292.2	292.3	292.4	292.5	292.2	
0.7	292.2	292.2	292.3	292.4	292.1	
0.8	292.1	292.2	292.2	292.2	292.1	
0.9	292	292.1	292.1	292.1	292.0	
1.0	292.0	292.0	292.0	292.1	292.0	

Table C.3 Recorded Brightness temperature for Bendix scanner at various altitudes when viewing asphalt surfaces at different temperatures against a grass background at a constant 293.2K. Sensor Zenith Angle = -135°

Target Temperature (K)	Detection Range (metres)
298.2	270
303.2	430
308.2	550
313.2	570

Table C.4 Estimated Detection Ranges for 20m² asphalt square against constant temperature (293.2K) grass backgrounds for different temperatures of asphalt.

Sensor Altitude (km)	Brightness Temperature (K)					
	a	b	c	d	e	f
0.1	292.1	290.1	290.6	286.8	291.4	288.5
0.2	292.2	291.4	290.4	288.9	291.2	290.1
0.3	292.2	291.8	290.2	289.5	291.1	290.6
0.4	292.2	292.0	290.0	289.6	291.0	290.7
0.5	292.2	292.1	289.8	289.6	290.9	290.7
0.6	292.2	292.1	289.7	289.5	290.8	290.6
0.7	292.1	292.1	289.6	289.4	290.6	290.6
0.8	292.1	292.0	289.4	289.3	290.5	290.5
0.9	292.0	292.0	289.3	289.2	290.4	290.4
1.0	292.0	292.0	289.2	289.2	290.3	290.3

a - No asphalt surface. Midlatitude Summer aerosol
b - Asphalt surface present. Midlatitude Summer aerosol
c - No asphalt surface. Midlatitude Winter aerosol
d - Asphalt surface present. Midlatitude Winter aerosol
e - No asphalt surface. SubArctic Summer aerosol
f - Asphalt surface present. SubArctic Summer aerosol

Table C.5 Estimated Brightness Temperature for grass (293.2K) and grass/asphalt (both 293.2K) surface configurations as functions of sensor altitude for different aerosols.

Sensor Field of View. (milliradians)	Brightness Temperature (K)
5	290.3
10	290.3
15	290.3
20	291.1
25	291.5
30	291.7
35	291.8
40	291.9
45	292.0
50	292.0

Table C.6 Variation in Estimated Brightness Temperature for a sensor at constant altitude, observing a $20m^2$ asphalt target against a grass background, both at 293.2K, for various detector fields-of-view.

References.

Banham P., (1993) Palm Microsystems U.K. Ltd, Private Communication

Cornette W.M., (1992) *Robust algorithm for correcting the layer problem in LOWTRAN*. App. Opt., **31**, no. 27, pp 5767-5769

Currell T.R., McComb T.J.L., and Turver K.E. (1991, unpublished) *Thermal Measurements, Albemarle Barracks 1991. Part 2 - Weather log*. Report TI/Durham 91/10, Durham.

Edwards P.J., McComb T.J.L., and Turver K.E. (1993, unpublished) *Analysis of the Ouston dataset for 1991 - APC data*. Report TI/Durham 93/8, Durham.

Greening C.P., Wyman M.J. (1970) *Experimental Evaluation of a Visual Detection Model*. Human Factors, **12**, no. 5, pp 435-445.

Hughes P.A., (1986) *Validation of a Model for Thermal Emission*. PhD Thesis, University of Durham.

Hughes P.A., McComb T.J.L., Rimmer A.B., Turver K.E., Rodgers M.L.B., Vickers A.F., Wright D.W. (1993) *A mathematical model for the prediction of temperature of man-made and natural surfaces*. Int. J. Remote Sensing, **14**, no. 7, pp 1383-1412

Johnson J. (1958) *Analysis of Image Forming Systems*. Proceedings of Image Intensifier Symposium, Fort Belvoir, Virginia, USA.

Kreiss W.T., Tchoubineh A., Lanich W.A., *Model for infrared sensor performance evaluation: applications and results. Optical Engineering,* **30**, no. 11, pp 1797-1803, (1991)

McComb T.J.L., Rimmer A.B., Rodgers M.L.B., Turver K.E., Vickers A.F. (1992) *A mathematical model for the prediction of temperature in a dry snow layer.* Cold Regions Science and Technology, **20**, pp 247-259

McComb T.J.L., Roberts I.D., and Turver K.E. (1991, unpublished) *Exploitation of the Durham Empirical Model - Analysis of the MCTC dataset.* Report TI/Durham 91/8, Durham.

McComb T.J.L., Roberts I.D., and Turver K.E. (1993, unpublished) *Analysis of the Ouston dataset for 1991 - Net data.* Report TI/Durham 93/9

Monteith J.L., Unsworth M.H. (1990) *Principles of Environmental Physics.* (2nd Edition) Published, Edward Arnold, London

Ratches J.A. (1976) *Static Performance Model for Thermal Imaging Systems.* Optical Engineering, **15**, no. 6, pp 525-530.

Richter R., (1991) *Model SENSAT-3 Technical Manual,* Revised Edition.

Rodgers M.L.B., (1992) Private Communication

Salvaggio C., Israel S., Kang Y.T., Bartholomew M.L., Pokrzywka D.M., Davis J.S., Duggin M.J. (1990) *Modelling scanning and staring imaging infrared sensors using a static performance model.* Int. J. Remote Sensing, **11**, no.12, pp 2311-2328.

Turver K.E. (1978, unpublished) *Measurements of target and background signatures in the far infrared spectral region,* S.C.R.D.E. Internal Report, Colchester, June 1978.

Turver K.E. (1986, unpublished) *Thermal emissions from natural and man-made objects,* Report TI/Durham 86/1, Durham.